

GDC-9545 (Giredestrant): A Potent and Orally Bioavailable Selective Estrogen Receptor Antagonist and Degradar with an Exceptional Preclinical Profile for ER+ Breast Cancer

Jun Liang,* Jason R. Zbieg, Robert A. Blake, Jae H. Chang, Stephen Daly, Antonio G. DiPasquale, Lori S. Friedman, Thomas Gelzleichter, Matthew Gill, Jennifer M. Giltane, Simon Goodacre, Jane Guan, Steven J. Hartman, Ellen Rei Ingalla, Lorn Kategaya, James R. Kiefer, Tracy Kleinheinz, Sharada S. Labadie, Tommy Lai, Jun Li, Jiangpeng Liao, Zhiguo Liu, Vidhi Mody, Neville McLean, Ciara Metcalfe, Michelle A. Nannini, Jason Oeh, Martin G. O'Rourke, Daniel F. Ortwine, Yingqing Ran, Nicholas C. Ray, Fabien Roussel, Amy Sambrone, Deepak Sampath, Leah K. Schutt, Maia Vinogradova, John Wai, Tao Wang, Ingrid E. Wertz, Jonathan R. White, Siew Kuen Yeap, Amy Young, Birong Zhang, Xiaoping Zheng, Wei Zhou, Yu Zhong, and Xiaojing Wang*

Cite This: <https://doi.org/10.1021/acs.jmedchem.1c00847>

Read Online

ACCESS |



Metrics & More

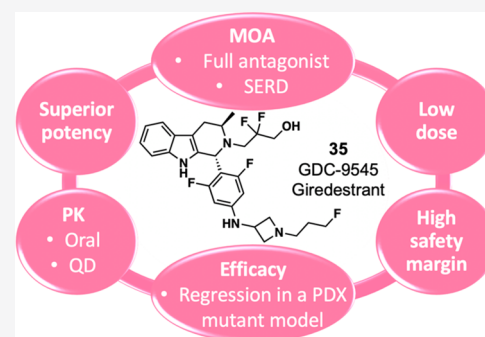


Article Recommendations



Supporting Information

ABSTRACT: Breast cancer remains a leading cause of cancer death in women, representing a significant unmet medical need. Here, we disclose our discovery efforts culminating in a clinical candidate, **35** (GDC-9545 or giredestrant). **35** is an efficient and potent selective estrogen receptor degrader (SERD) and a full antagonist, which translates into better antiproliferation activity than known SERDs (**1**, **6**, **7**, and **9**) across multiple cell lines. Fine-tuning the physiochemical properties enabled once daily oral dosing of **35** in preclinical species and humans. **35** exhibits low drug–drug interaction liability and demonstrates excellent *in vitro* and *in vivo* safety profiles. At low doses, **35** induces tumor regressions either as a single agent or in combination with a CDK4/6 inhibitor in an ESR1^{Y537S} mutant PDX or a wild-type ER α tumor model. Currently, **35** is being evaluated in Phase III clinical trials.



INTRODUCTION

In women, breast cancer is the most commonly diagnosed cancer (24.5% of total cases) and the leading cause of cancer death (15.5%) among all cancers in 2020 worldwide,¹ representing a critical unmet medical need and a global healthcare priority.² Breast cancer is the most frequently occurring cancer among women, affecting one out of every eight women in their lifetime.³ Approximately 70% of all breast cancers express estrogen receptor alpha (ER α),⁴ making it a prime target for treatment.^{5,6} Standard of care therapies for ER+ breast cancer patients include three major classes of drugs: (1) those that directly target ER α , (2) aromatase inhibitors (AIs) that reduce the level of estrogens, and (3) cyclin-dependent kinases 4 and 6 (CDK4/6) cell-cycle checkpoint inhibitors.^{7–9} Fulvestrant (**1**, Figure 1) was approved in the early 2000s as a full ER α antagonist and subsequently identified as a selective estrogen receptor degrader (SERD).^{10,11} However, the poor druglike properties¹² necessitating intramuscular administration¹¹ of **1** limit its target occupancy¹³ and may consequently limit its efficacy.¹⁴ Tamoxifen (**2**) was approved in the 1970s as a selective

estrogen receptor modulator (SERM).^{15,16} Its partial agonism has been linked to a higher risk of developing endometrial carcinoma¹⁷ and has been also implicated in the development of breast cancer resistance.^{18,19} In recent years, hot-spot mutations of the ESR1 gene encoding ER α were discovered resulting in constitutively active ER α activity and resistance to early line endocrine treatments.^{20–23} These endocrine therapy resistant tumors nevertheless depend on ER α for growth and survival, as evidenced by their sensitivity to **1**. Given the high unmet medical need for treating ER+ breast cancer, there has been a surge of drug discovery effort in identifying orally bioavailable SERDs (**3–9**) to improve oral exposure, efficacy, and safety in the clinic.^{24–32}

Received: May 10, 2021

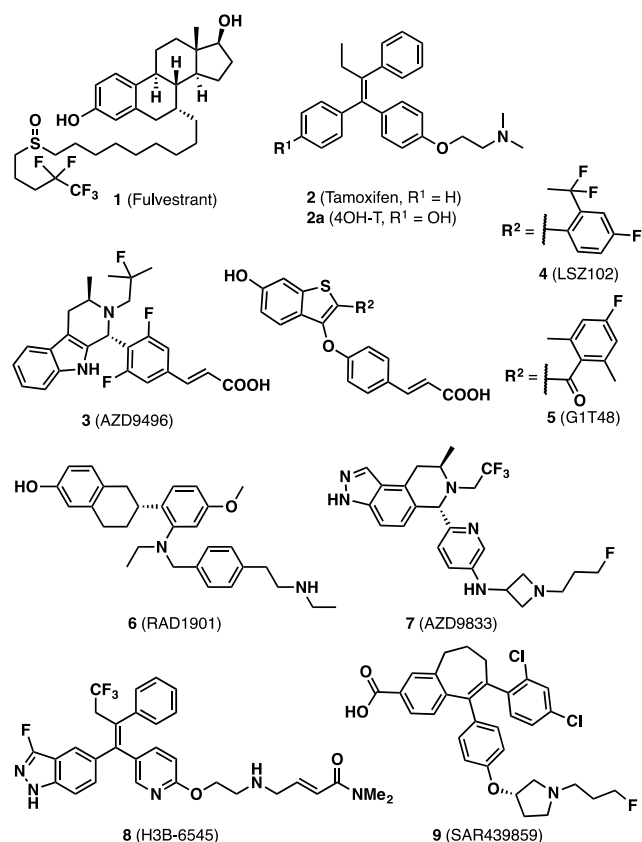


Figure 1. Approved or selected clinical stage SERDs or SERMs.

We were among the first to test an oral SERD in patients, namely, GDC-0810 (**10**, Table 1).^{33–35} Despite good oral bioavailability observed in preclinical species such as rats, **10** is significantly less potent than **1** in antagonist (IC₅₀ 5.31 vs 0.25 nM), degradation (DC₅₀ 0.74 vs 0.12 nM), and antiproliferation (EC₅₀ 17 vs 2.4 nM) assays (Table 1). In addition, **10** is a less efficient degrader than **1** as indicated by the saturation infinity (*S*_{inf}) values (96% vs 103%) which were shown to correlate with antiproliferative efficiency and *in vivo* efficacy.³³ Of note is that tamoxifen (**2**) and its active metabolite 4-hydroxy tamoxifen (4-OH-T, **2a**) are not considered ERα degraders based on Western blot assay data. However, they do possess modest degradation efficiency (*S*_{inf} = 56% and 62%, respectively) in an MCF-7 immunofluorescent (IF) cellular degrader assay. This may indicate the improved sensitivity of the IF compared to Western blot assay for reasons that are not yet understood. Despite this discrepancy, the general rank ordering of compounds' degradation efficiencies by Western blot and IF assays were consistent in our hands. Therefore, one of our goals was to maximize the degradation efficiency (*S*_{inf}) utilizing the IF assay, which is higher throughput than Western blot. In addition to being a partial agonist in rat uterus, **10** was later found to have partial agonism in breast cancer cell lines similar to SERMs **2** and **2a**,³⁶ hence **10** is labeled as selective estrogen receptor degrader/modulator (SERD/M) hereafter. The clinical development of **10** was halted given the totality of data. Our second oral SERD clinical candidate, GDC-0927 (**11**),³⁷ exhibited better potencies (3–8-fold) in all three cellular assays and also higher ligand-lipophilicity efficiency (LLE), indicating better drug-likeness³⁸ than **1**. However,

Table 1. Our Previously Disclosed SERDs Compared to Approved SERM or SERD Drugs

ID	Antag IC ₅₀ (nM) ^a	Degrad DC ₅₀ (nM)/ <i>S</i> _{inf} ^b	Proli EC ₅₀ (nM) ^c	<i>In vitro</i>			<i>In vivo</i>		<i>LogD</i> ⁱ	<i>LLE</i> ^j
				Sol ^d	H/RHep CL _{hep} ^e	<i>P</i> _{app} ^f	Rat CL _g ^g	<i>F</i> % ^h		
1	0.25	0.12/103%	2.4	3	15/29	nt	nt	nt	>5	<3.6
2	58	91/56%	>200	1	12/33	0.2	95	69	4.2	2.5
2a	1.36	0.13/62%	3.5	31	14/32	n/a	nt	nt	4	4.5
10	5.31	0.74/96%	17	19	15/6	2.3	40	30	3.8	4.0
11	0.10	0.03/97%	0.3	47	16/46	4.6	85	17	2.9	6.6
12	0.53	0.08/95%	1.0	10	6/29	n/a	34	31	4.0	5.0
13	0.14	0.05/100%	0.7	1	7/31	0.4	19	31	4.8	4.4

^aCellular antagonist assay measuring the level of luciferase expression in T-47D wild-type cells. Geometric mean values are shown. 95% Confidence intervals (when *n* ≥ 3) can be found in Table S2 in the Supporting Information. ^bCellular degradation assay measuring the fluorescence intensity of tagged ERα in MCF-7 wild-type cells. Geometric mean values are shown. 95% Confidence intervals (when *n* ≥ 3) can be found in Table S2 in the Supporting Information. ^cCellular proliferation assay measuring CellTiter-Glo in MCF-7 breast cancer cells. Geometric mean values are shown. 95% Confidence intervals (when *n* ≥ 3) can be found in Table S2 in the Supporting Information. ^dMeasured kinetic solubility in μM at pH 7.4. ^eH/RHep, projected hepatic clearance using human or rat hepatocytes (mL/min/kg). ^f*P*_{app}, measured permeability using Madin-Darby Canine Kidney (MDCK) epithelial cell lines, A to B (×10^{−6} cm/s); n/a, not available due to low mass recovery; nt, not tested. ^gTotal clearance in rat *in vivo* (mL/min/kg). Compounds were dosed at 1 mg/kg in a solution of 45/55 PEG400/water for **10**, 35/65 PEG400/water for **11**, 10/60/30 DMSO/PEG400/water for **2**, **12**, and **13**. ^hRat oral bioavailability calculated using (AUC_{oral}/AUC_{iv}) × (dose_{iv}/dose_{oral}) × 100. Compounds were dosed at 5 (**2**, **10**, **11**) or 1 (**12** and **13**) mg/kg in a suspension of MCT in water. ⁱMeasured distribution-coefficient at pH 7.4. ^jLigand-lipophilicity efficiency (LLE), pEC₅₀ – log *D*.

clinical development of **11** was halted in 2017 due to low oral exposure and consequently high pill burden in clinical trials.

We then discovered a distinct series of oral SERDs represented by **12** and **13**³⁹ with degradation efficiencies and potencies in antagonist, degradation, and proliferation assays comparable to or improved over **1** and **11**. Notably, the oral exposures of **12** and **13** were greatly improved over **11**. However, given the relatively high lipophilicity ($\log D \geq 4$), **12** and **13** proved to have low solubility and consequently reduced LLE and drug-likeness. Herein, we report our lead optimization effort in discovering a best-in-class oral SERD clinical candidate with a dual mechanism of action as a full ER α antagonist and a strong/efficient degrader, together with a superior physicochemical, pharmacokinetic, and safety profile.

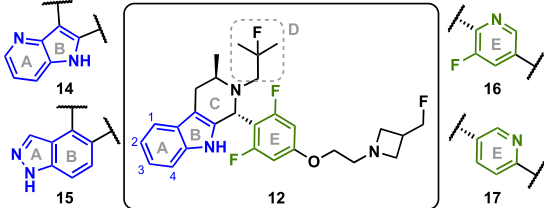
RESULTS AND DISCUSSION

Historically, it has been extremely challenging to lower the lipophilicity of ER α ligands while maintaining potency⁴⁰ (Table S1 in the Supporting Information) due to the lipophilic nature of the ER α ligand binding pocket. Given this, we decided to take a systematic approach to add polarity and consequently improve the physicochemical properties without sacrificing potency. First, we reduced the lipophilicity by introducing an aromatic nitrogen in various locations using **12** as a template. To frame the discussion, we have applied the ring naming system (A–D) of estradiol to **12** (Table 2) based on the predicted and observed binding modes. Aza analogue **14** with a pyridyl nitrogen at the 1-position of the A-ring (Table 2) was 3- to 7-fold less potent than **12** in all three

cellular assays and was also more labile in human and rat liver microsomes (LM). Analogues with a pyridyl nitrogen at the 2- to 4-positions of the A-ring could not be synthesized, most likely due to the substantially reduced electron density of the AB-rings which hampered the formation of the C-ring using the requisite Pictet–Spengler reaction.⁴¹ Inspired by the indazole moiety in **10**, we made analogue **15** by flipping the AB-ring and adding an extra aromatic nitrogen. This compound had slightly improved cellular potencies and improved degradation efficiency over **12**, at a cost of metabolic stability in human and rat liver microsomes as indicated by higher hepatic clearance (CL_{hep}). In addition, **15** had low solubility and slightly lower ligand-lipophilicity efficiency (LLE, 4.6 vs 5.0) than **12**. Replacing one of the C–F substitutions in the E-ring of **12** with a pyridyl nitrogen (**16**) drastically eroded antagonist and antiproliferation potencies, despite an increase of solubility. Adding a pyridyl nitrogen while removing the two fluorine atoms in the E-ring of **12** resulted in an analogue (**17**) with comparable potencies and liver microsomes stabilities along with improved solubility and LLE. Thus, among this set of analogues with aza core changes, **17** was identified as the most improved analogue over **12**.

Next, we explored introducing polarity onto the side chain occupying the D-ring area. In earlier work, we learned that substituting the tetrahydrocarboline (THC) alkyl amine with carbonyl or sulfonyl groups significantly improved the drug-likeness but at the cost of potencies (manuscript submitted). Therefore, we focused on the alkyl side chains themselves. In a previous report,²⁴ a lipophilic hole (Leu525:Leu384) in ER α was discovered that was occupied by a “magic methyl” group (highlighted in red in **12** in Table 3). There was a 100- to 1000-fold potency gain with a concurrent change from H and OH to two methyl groups on the β -carbon of the THC alkyl amine. Indeed, when the two methyl groups in **12** were connected through an oxygen atom forming an oxetane ring (**18**), there was a 10-fold decrease in the antagonist activity and a decrease in degradation efficiency by 5%. However, solubility (10-fold) and LLE (+1.5) increased relative to **12**. Encouraged by the improved physicochemical properties, we retained the oxetane moiety while incorporating the “magic methyl” group (**19**). We observed comparable antagonist potency, slightly improved degradation and antiproliferation potencies, and improved LLE (+1.1) from **12** to **19**. However, an erosion of the liver microsomes stability was observed for **19**. Further profiling of **19** showed high metabolic instability in rat hepatocytes, which was corroborated *in vivo* with a total clearance above hepatic blood flow in a rat pharmacokinetic (PK) study. Another strategy was to replace the methyl groups in **12** with fluorine atoms (**20** and **21**). We reasoned that this might temper the basicity of the THC alkyl amine to be more compatible with the lipophilic ER α binding site while lowering lipophilicity, resulting in higher LLE. Indeed, the loss of potency by removing the “magic methyl” group seemed to be mitigated, resulting in comparable potencies among **20**, **21**, and **12**. In addition, both **20** and **21** had improved solubility and LLE over **12**. Based on a cocrystal structure of **12** with ER α ,³⁹ we noticed residue His524 was in the vicinity of the D-ring side chain. A primary alcohol was therefore installed to interact with this residue (Table 3, **22** and **23**), resulting in a slight loss of degradation efficiency (3%) but a comparable or slight gain in all potencies compared to **12**. Interestingly, antagonist and antiproliferation potencies did not always correlate, most likely due to the different cell lines used for the

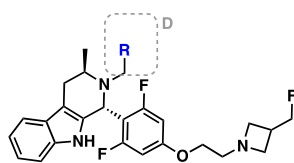
Table 2. Introducing Polarity in either the A- or E-Ring to Increase Ligand-Lipophilicity Efficiency



ID	Antag IC ₅₀ ^a (nM)	Degrad DC ₅₀ ^b (nM)/S _{inf}	Proli EC ₅₀ ^c (nM)	Sol ^d	H/RLM CL _{hep} ^e	LLE ^f
12	0.5	0.08/95%	1.0	10	10/29	5.0
14	3.6	0.26/94%	2.8	75	19/44	4.7
15	0.2	0.06/99%	0.8	1	17/44	4.6
16	12	0.14/93%	10	215	15/26	5.0
17	0.7	0.03/97%	0.9	33	12/38	5.5

^aCellular antagonist assay measuring the level of luciferase expression in T-47D wild-type cells. Geometric mean values are shown. 95% Confidence intervals (when $n \geq 3$) are in Table S2 in the Supporting Information. ^bCellular degradation assay measuring the fluorescence intensity of tagged ER α in MCF-7 wild-type cells. Geometric mean values are shown. 95% Confidence intervals (when $n \geq 3$) are in Table S2 in the Supporting Information. ^cCellular proliferation assay measuring CellTiter-Glo in MCF-7 breast cancer cells. Geometric mean values are shown. 95% Confidence intervals (when $n \geq 3$) are in Table S2 in the Supporting Information. ^dMeasured kinetic solubility in μM at pH 7.4. ^eH/RLM, projected hepatic clearance using human or rat liver microsomes (mL/min/kg). ^fLigand-lipophilicity efficiency (LLE), $pEC_{50} - \log D$.

Table 3. Optimizing Nitrogen Substituents on the THC to Improve Cellular Potencies, Degradation Efficiencies, Solubility, and LLE



ID	R	Antag IC ₅₀ (nM) ^a	Degrad DC ₅₀ (nM)/S _{inf} ^b	Proli EC ₅₀ (nM) ^c	<i>In vitro</i>		LLE ^f
					Sol ^d	H/RLM CL _{hep} ^e	
12		0.5	0.08/95%	1.0	10	10/29	5.0
18		6.0	0.11/90%	0.6	112	12/29	6.5
19		0.5	0.02/96%	0.4	35	15/37	6.1
20		0.3	0.07/96%	1.0	71	11/26	5.8
21		0.8	0.08/97%	0.7	21	11/27	5.4
22		0.4	0.03/92%	0.2	111	14/27	7.0
23		0.8	0.08/92%	0.5	81	10/26	6.9
24		2.1	0.63/93%	9.8	195	<4/<6	7.9
25		0.4	0.09/94%	1.2	10	13/32	4.8
26		0.1	0.02/97%	0.6	115	12/26	6.5

^aCellular antagonist assay measuring the level of luciferase expression in T-47D wild-type cells. Geometric mean values are shown. 95% Confidence intervals (when $n \geq 3$) are in Table S2 in the Supporting Information. ^bCellular degradation assay measuring the fluorescence intensity of tagged ER α in MCF-7 wild-type cells. Geometric mean values are shown. 95% Confidence intervals (when $n \geq 3$) are in Table S2 in the Supporting Information. ^cCellular proliferation assay measuring CellTiter-Glo in MCF-7 breast cancer cells. Geometric mean values are shown. 95% Confidence intervals (when $n \geq 3$) are in Table S2 in the Supporting Information. ^dMeasured kinetic solubility in μ M at pH 7.4. ^eH/RLM, projected hepatic clearance using human or rat liver microsomes (mL/min/kg). ^fLigand-lipophilicity efficiency (LLE), $\text{pEC}_{50} - \log D$.

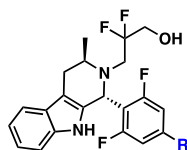
study (T-47D and MCF-7 for the antagonist and proliferation assay, respectively). These results demonstrated again that SERDs can have different phenotypes in different cell lines.⁴² Since the alcohol was tolerated, we also probed carboxylic acid and nitrile substitutions as in **24** and **25**. Results showed a consistent loss of potencies (4- to 10-fold) across the three cellular assays despite improvements in solubility, liver microsomes stability, and LLE from **12** to **24**. The decreases in cellular potencies of **24** were most likely due to the loss of binding activity (data not shown). The nitrile analogue **25** was comparable to **12** in all aspects, except with a slightly lower LLE.

Based on the above structure activity relationships (SAR), we proposed a difluoropropyl alcohol side chain, which would have multiple benefits including removing a chiral center, tempering basicity of the THC alkyl amine, reducing lipophilicity, and strengthening a potential hydrogen bond with His524 due to a more polarized terminal hydroxy group. Gratifyingly, the resulting compound (**26**) had improved potencies (2- to 5-fold) in all three assays, improved degradation efficiency (+2%), and improved solubility (10-fold) and LLE (+1.5) over **12**. Liver microsomes stability was similar between **12** and **26**. The difluoropropyl alcohol side chain as in **26** was therefore identified as the optimal THC nitrogen substituent.

We next interrogated the side chain appended to the 4-position of the 2,6-difluorophenyl ring. Previous studies revealed large impacts in degradation efficiency with small

structural changes.^{37,39} Replacing an ether linkage (**26**) with an aniline (**27**, Table 4) resulted in slight decreases in antagonist and degradation potencies (2- to 5-fold) and degradation efficiency (−3%), while antiproliferation potency, liver microsomes stability, solubility, and LLE were maintained or slightly increased. Adding a carbonyl (**28**) did not improve the antagonist activity substantially compared to **27** but had a detrimental effect on the degradation efficiency (57% vs 94%). In fact, the degradation efficiency of **28** (57%) was similar to that of **2**, a nondegrader by Western blot. This degradation-efficiency cliff demonstrated the sensitivity of degradation to structural changes in this part of the molecule. Opening up the four-membered azetidine to a linear chain such as in **29** and **30** also resulted in a significant loss of degradation efficiency (−8% and −7%, respectively) compared to **26**. We also studied rigidification with a five-membered pyrrolidine ring (**31** and **32**). The degradation efficiencies of **31** and **32** were slightly higher (2%) than **26**, however at a cost of a 6- to 8-fold reduction in degradation potencies. Ring contraction to a four-membered azetidine (**33**) restored the degradation potency to a level same as that of **26**, while further improving the degradation efficiency (4%). Replacing the terminal fluorine atom with a hydroxy group (**34**) eroded the degradation efficiency (−17%) compared to **26**, reinforcing the steep activity cliffs. Changing the linker from oxygen to amine yielded **35**, which was 3-fold more potent as an antagonist than **26**, proving to be the most potent compound in the antagonist assay. In addition to its high potency as an antagonist, **35**

Table 4. Interrogation of the Pendent Degradation Side Chain for Maximum Degradation Efficiency



ID	R	Antag IC ₅₀ (nM) ^a	Degrad DC ₅₀ (nM)/S _{inf} ^b	Prolif EC ₅₀ (nM) ^c	In vitro		LLE ^f
					Sol ^d	H/RLM CL _{hep} ^e	
26		0.12	0.02/97%	0.6	115	12/26	6.5
27		0.23	0.10/94%	0.6	129	13/22	6.9
28		0.16	0.14/57%	2.1	91	12/25	5.7
29		nt	0.25/89%	0.9	191	6/10	6.6
30		nt	0.27/90%	0.6	199	7/<6	7.0
31		nt	0.12/99%	0.3	35	15/35	6.2
32		nt	0.16/99%	0.3	80	11/26	6.5
33		0.13	0.02/101%	0.5	35	14/32	6.0
34		0.08	0.03/80%	0.6	163	9/10	5.4
35		0.05	0.03/101%	0.4	135	11/19	6.5
36		0.09	0.02/100%	0.8	42	12/25	4.5
37		0.29	0.17/94%	1.1	18	13/26	5.6
38		0.09	0.02/97%	0.6	95	9/15	6.5
39		0.07	0.14/62%	1.4	128	6/10	7.0
40		0.89	0.78/96%	11	104	6/10	6.6

^aCellular antagonist assay measuring the level of luciferase expression in T-47D wild-type cells. nt, not tested. Geometric mean values are shown. 95% Confidence intervals (when $n \geq 3$) are in Table S2 in the Supporting Information. ^bCellular degradation assay measuring the fluorescence intensity of tagged ER α in MCF-7 wild-type cells. Geometric mean values are shown. 95% Confidence intervals (when $n \geq 3$) are in Table S2 in the Supporting Information. ^cCellular proliferation assay measuring CellTiter-Glo in MCF-7 breast cancer cells. Geometric mean values are shown. 95% Confidence intervals (when $n \geq 3$) are in Table S2 in the Supporting Information. ^dMeasured kinetic solubility in μ M at pH 7.4. ^eH/RLM, projected hepatic clearance using human or rat liver microsomes (mL/min/kg). ^fLigand-lipophilicity efficiency (LLE), pEC₅₀ – log D.

maintained high degradation and antiproliferation potency/efficiency, solubility, and LLE. Adding a fluorine atom to the side chain terminus (36), introducing branching (37), or removing the terminal fluorine atom (38) yielded inferior compounds. Replacing the terminal fluorine atom with a hydroxy group (39) also eroded the degradation efficiency (S_{inf} = 62%). Finally, returning to the acrylic acid side chain (40), we noted a marked decrease in potencies across three cell assays (7- to 39-fold) compared to 26. From this set of SARs, 33 and 35 were identified as top leads, which not only achieved the maximum degradation efficiency but also struck the desired balance between potency and drug-likeness/LLE.

From the cocrystal structure of 35 and ER α (Figure 2), we observed three key polar interactions. First, we observed an ionic interaction from the charged azetidine nitrogen (with a measured pK_a of 8.1) to the side chain of Asp351 in helix 3 (H3) at a 2.9 Å distance. This strong ionic interaction with Asp351 rendered 35 potent against ESR1 hot-spot mutant Y537S and compared favorably against 1 in both mutant

degradation and proliferation assays (Table S3 in the Supporting Information). Second, consistent with our initial design, the primary alcohol from the D-ring side chain of 35 makes a strong hydrogen bonding (HB) interaction with His524 of helix 11 (H11) at a 2.5 Å distance. As a result, H11 packs more closely around the ligand 35. Third, a weak HB interaction from the indole NH of the THC core to the backbone carbonyl oxygen of Leu346 in H3 at a 3.6 Å distance further strengthened the ligand interactions with H3. In addition, there are multiple van der Waals interactions between protein and ligand throughout the binding pocket and multiple noncanonical HB interactions from the ligand to the receptor (Glu353, Met421, Gly521, Asn532, and Val533, Figure S3 in the Supporting Information). The loop connecting H11 and H12 was largely disordered in this structure. Compared to the cocrystal structure of 11, Glu353 in 35 rotated by 52° in order to accommodate the nonpolar phenyl group in 35. Such rotation of Glu353 enabled a noncanonical HB interaction between the CH group of the phenyl ring in 35 and the oxygen

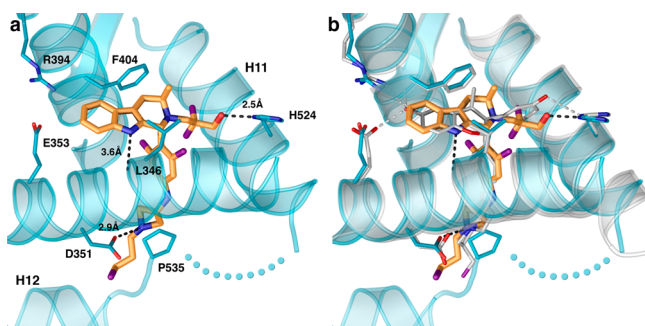
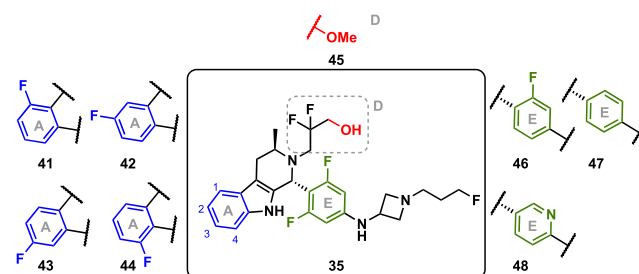


Figure 2. Binding environment of 35. (a) Co-crystal structure of ER α (blue ribbon schematic) with 35 (orange carbons, PDB code 7MSA) bound in the ligand binding pocket showing the three hydrogen bonds formed between the protein and ligand as well as a subset of the amino acid side chains lining the site. The loop connecting helices 11 (H11) and 12 (H12) was disordered in the structure and is represented by a blue dotted arc. (b) While 35 forms a hydrogen bond to the backbone of L346, antagonist 11 (gray carbons, PDB code 6PFM)⁴³ forms the canonical steroid hydrogen bonds with E353 and R394.

atom of Glu353 at a 2.7 Å distance. Because of this extra phenyl ring of 35 in place of the phenol OH of 11, there is an added van der Waals interaction for 35 with Leu387 in H4/5. In addition, 35 has extra HB interactions in both the A- and D-ring areas with Leu346, Met421, and Gly521 and stronger HBs with His524 and Asp351 than 11. All of these interactions likely contributed to enhanced potency of 35 compared to 11. The absolute stereochemistry of 35 was unambiguously confirmed to be *R* at both stereocenters using small molecule X-ray crystal structure (Table S6 and Figure S4 in the Supporting Information).

To ensure the selection of a best-in-class candidate, we further studied close-in analogues of 35 with one-point modifications. To investigate whether the edge-to-face π interaction of Phe404 to the THC core could be further enhanced by modulating the electrostatic potential, we designed and made the fluorinated analogues 41–44 (Table 5). All four analogues 41–44 maintained excellent degradation potency, with 41 having slightly improved degradation efficiency (+2%) compared to 35. However, there was a slight erosion of antagonist potency for 41–44, especially for 41 (3-fold less than 35) and 44 (5-fold less than 35). Similarly, there was a slight decrease in antiproliferation potency, solubility, and LLE from 35 to 41–44. Methylation of the primary alcohol in the D-ring area of 35 resulted in 45. Unfortunately, 45 exhibited lower potency across all three cellular assays, lower solubility, slightly higher LM metabolism, and lower LLE than 35, confirming the importance of the alcohol for both potency and physicochemical properties. Interestingly, removal of fluorine atoms in the E-ring (46 and 47) resulted in significant erosion of antagonist potency, 20-fold and 12-fold less than 35, respectively. The lower antagonist potency, lower antiproliferation potency, and lower LLE of 46 and 47 rendered both molecules less attractive than 35, despite their comparable degradation potency/efficiency, solubility, and LM stability to 35. Given the encouraging results for 17 discussed earlier, pyridyl analogue 48 yielded a surprising potency cliff. We hypothesized that this was due to the intramolecular hydrogen bond of aniline NH with the pyridyl nitrogen which positioned the azetidine degradation side chain unfavorably.

Table 5. One-Point Optimization of 35 (GDC-9545) to Maximize Potency and LLE



ID	Antag IC ₅₀ (nM) ^a	Degrad DC ₅₀ (nM)/S _{int} ^b	Proli EC ₅₀ (nM) ^c	<i>In vitro</i>		LLE ^f
				Sol ^d	H/RLM CL _{hep} ^e	
35	0.05	0.03/101%	0.4	135	11/19	6.5
41	0.15	0.04/103%	0.5	92	12/19	6.0
42	0.06	0.03/101%	0.5	91	10/14	6.0
43	0.09	0.02/101%	0.7	110	9/15	5.6
44	0.25	0.03/100%	1.0	110	11/16	5.3
45	0.16	0.10/102%	1.4	35	13/27	5.1
46	0.98	0.02/102%	2.7	112	10/10	5.7
47	0.60	0.04/102%	2.8	173	10/17	5.6
48	>1000	>1000/-	>200	114	6/23	<6.4

^aCellular antagonist assay measuring the level of luciferase expression in T-47D wild-type cells. Geometric mean values are shown. 95% Confidence intervals (when $n \geq 3$) are in Table S2 in the Supporting Information. ^bCellular degradation assay measuring the fluorescence intensity of tagged ER α in MCF-7 wild-type cells. Geometric mean values are shown. 95% Confidence intervals (when $n \geq 3$) are in Table S2 in the Supporting Information. ^cCellular proliferation assay measuring CellTiter-Glo in MCF-7 breast cancer cells. Geometric mean values are shown. 95% Confidence intervals (when $n \geq 3$) are in Table S2 in the Supporting Information. ^dMeasured kinetic solubility in μ M at pH 7.4. ^eH/RLM, projected hepatic clearance using human or rat liver microsomes (mL/min/kg). ^fLigand-lipophilicity efficiency (LLE), $\text{pEC}_{50} - \log D$.

Based on the totality of data, we selected 41–43 from this group of analogues for further characterization.

Next, we compared the five top leads (33, 35, and 41–43) to the FDA approved drug 1 and the prototypic THC analogue 13 in *in vitro* and *in vivo* drug metabolism and pharmacokinetics (DMPK) studies (Table 6). Sorted by ascending LLE in Table 6, it was clear that all five top leads had higher LLE/drug-likeness than 1 and 13, with analogue 35 being the best. Correspondingly, these top leads showed lower lipophilicity, higher solubility, and higher permeability than 1 and 13. With decreasing lipophilicity, all five top leads were less plasma protein bound, resulting in lower unbound clearance than 13 in rat without sacrificing oral bioavailability. In addition, the antagonist, degradation, and antiproliferation potencies of these top leads were better than 1 and comparable or better than 13. With this data in hand, we progressed 35 and 42 to further studies.

We next compared the cytochrome P450 (CYP) inhibition profiles of 35 and 42 (Table 7). CYP3A family, particularly CYP3A4, is by far the most abundant CYP enzyme in humans, mediating the metabolism of approximately half of all marketed drugs.⁴⁴ Perturbation of CYP enzyme activities may incur undesirable drug–drug interactions. 35 exhibited low to moderate reversible inhibition of CYP3A4 with 42 being

Table 6. Candidate Selection (33, 35, 41–43) through the Multiparameter Comparison with 1 and 13

ID	LLE ^a	LogD ^b	Antag IC ₅₀ (nM) ^c	Degrad DC ₅₀ (nM)/S _{inf} ^d	Proli EC ₅₀ (nM) ^e	In vitro			In vivo	
						SoI ^f	H/RHep CL _{hep} ^g	P _{app} ^h	Rat CL _t /CL _u ⁱ	F% ^j
1	<3.6	>5	0.25	0.12/103%	2.4	3	15/29	nt	nt	nt
13	4.4	4.8	0.14	0.05/100%	0.69	1	8/29	0.4	19/19300	31
43	5.6	3.5	0.09	0.02/101%	0.72	110	9/15	1.9	19/9300	36
33	6.0	3.4	0.13	0.02/101%	0.48	35	16/41	6.7	18/2129	26
41	6.0	3.3	0.15	0.04/103%	0.51	92	12/23	0.9	27/13650	22
42	6.0	3.4	0.06	0.03/101%	0.45	91	10/15	2.3	18/1475	35
35	6.5	2.9	0.05	0.03/101%	0.36	135	12/23	3.0	21/3533	41

^aLigand-lipophilicity efficiency (LLE), $pEC_{50} - \log D$. ^bMeasured distribution-coefficient at pH 7.4. ^cCellular antagonist assay measuring the level of luciferase expression in T-47D wild-type cells. ^dCellular degradation assay measuring the fluorescence intensity of tagged ER α in MCF-7 wild-type cells. ^eCellular proliferation assay measuring CellTiter-Glo in MCF-7 breast cancer cells. ^fMeasured kinetic solubility in μ M at pH 7.4. ^gH/RHep, projected hepatic clearance using human or rat hepatocytes (mL/min/kg). ^hP_{app}, measured permeability using Madin–Darby canine kidney (MDCK) epithelial cell lines, A to B ($\times 10^{-6}$ cm/s); nt, not tested. ⁱCL_t, total clearance in rat *in vivo* (mL/min/kg). CL_u, unbound clearance in rat *in vivo* (mL/min/kg). Compound was dosed at 1 mg/kg in a solution of 10/60/30 DMSO/PEG400/water. ^jRat oral bioavailability calculated using $(AUC_{oral}/AUC_{iv}) \times (dose_{iv}/dose_{oral}) \times 100$; compound was dosed at 1 mg/kg in a suspension of MCT in water.

Table 7. In Vitro Reversible and Time Dependent Inhibition (TDI) of CYPs by 35 and 42

	CYP reversible IC ₅₀ (μ M) ^a					CYP TDI %AUC shift ^b					
	3A4(M)	3A4(T)	2C9	2C19	2D6	3A4(M)	3A4(T)	1A2	2C9	2C19	2D6
35	6.5	26	>10	>10	>10	-0.9	-4.0	1.0	19	1.2	8.1
42	2.7	1.6	>10	>10	>10	2.0	-39	-6.1	12	13	0.9

^aReversible CYP inhibition assay, using either midazolam (M) or testosterone (T) as the probe substrate for CYP3A4. ^bTDI of CYP measuring the percentage of AUC shift, using midazolam (M) or testosterone (T) as a probe for CYP3A4.

Table 8. Selectivity and In Vitro Safety Profiles of 35 and 42

Assay ^a		35	42
Kinase selectivity ^b	Binding% > 40% at 10 μ M	No hits	No hits
HNR selectivity ^c	Inhibition% > 30% at 1 μ M	No hits	No hits
Secondary pharmacology ^d	Binding% > 75% at 10 μ M	2	8
In vitro cardiac safety pharmacology	hERG IC ₅₀ (μ M) ^e	6.1	2.8
	hNa _v 1.5 inh% at 10 μ M ^f	16.7%	14.0%
	hCa _v 1.2 inh% at 10 μ M ^g	15.7%	10.7%
Genotoxicity	AMES	negative	negative
	In vitro MNT	negative	negative

^aSee the Supporting Information for assay methods and details. ^bA panel of 220 kinases. ^cA panel of 23 human nuclear receptors (HNR).

^dSecondary pharmacology panel including 42 ion channels, G protein-coupled receptors, transporters, and enzymes. ^ehERG potassium channel patch clamp assay. ^fhNa_v1.5 channel inhibition at 10 μ M (resting). ^ghCa_v1.2 channel inhibition at 10 μ M.

more potent than 35. It is worth noting that both 35 and 42 did not block the function of other CYP enzyme isoforms including 2C9, 2C19, 2D6 (IC₅₀ > 10 μ M). In addition, both 35 and 42 were not time-dependent inhibitors against CYP3A4, 1A2, 2C9, 2C19, and 2D6, suggesting there was low potential for drug–drug interaction liability.

Both 35 and 42 were highly selective against a panel of 220 kinases and 23 human nuclear receptors (Table 8). Both were negative in *in vitro* genotoxicity studies, including the bacterial reverse mutation assay (AMES) and micronucleus test (MNT). Furthermore, 35 and 42 showed minimal activity (<20% inhibition at 10 μ M) against hNa_v1.5 and hCa_v1.2 ion channels. However, consistent with the slightly higher lipophilicity of 42 than 35, 42 incurred more off-target activity than 35 when tested against a secondary pharmacology panel

consisting of 42 receptors, ion channels, transporters, and enzymes (8 hits for 42 vs 2 hits for 35). Moreover, 42 was 2-fold more potent against the human ether-à-go-go-related gene (hERG) potassium ion channel than 35. In light of the data described above, we decided to profile 35 more extensively as a potential development candidate.

The absorption, distribution, metabolism, and excretion (ADME) profile of compound 35 is summarized in Table 9. Predicated hepatic clearance in LM and hepatocytes (Hep) was mostly moderate across four preclinical species and humans, with the exception of low Hep CL_{hep} in dogs and high Hep CL_{hep} in cynos. The *in vivo* clearance was moderate in rats and cynos and low in dogs. The oral bioavailability (F %) was 17% in cynos, 41% in rats, and 55% in dogs when administered as a suspension with amorphous free base of 35 at 1 mg/kg.

Table 9. Preclinical ADME Profiling of 35

Species	<i>In vitro</i>		<i>In vivo</i>			
	LM CL _{hep} ^a	Hep CL _{hep} ^b	CL ^c	F% ^d	V _{ss} ^c	T _{1/2} ^c
mouse	52	33	--	--	--	--
rat	19	23	21	41 ^e – 65 ^f	15	8
dog	13	<7.8	3	55 ^e	5.1	24
cyno	22	31	19	17 ^e – 29 ^f	9.4	7.3
human	11	12	--	--	--	--

^aProjected hepatic clearance using liver microsomes (mL/min/kg).

^bProjected hepatic clearance using hepatocytes (mL/min/kg). ^cTotal clearance *in vivo* (CL, mL/min/kg); volume of distribution at steady state (V_{ss}, L/kg); half-life (T_{1/2}, h); 35 was dosed at a 1 mg/kg dose in a solution of 10/60/30 DMSO/PEG400/water in rats (n = 3), or in a solution of 10/60/30 EtOH/PEG400/water in dogs (n = 3) or cynomolgus (cyno) monkey (n = 3). ^dF % is oral bioavailability with 35 dosed in a suspension of MCT. ^eAmorphous free base of 35 in a 1 mg/kg dose (n = 3). ^fCrystalline tartrate salt of 35 in a 100 mg/kg dose (n = 3).

There was a slight increase in F % in both rats and cynos using a crystalline tartrate salt of 35 at a 100 mg/kg dose. The volume of distributions at steady state (V_{ss}) in rats, dogs, and cynos were high resulting in half-lives (T_{1/2}) between 8 and 24 h. Based on these preclinical data, low to moderate clearance and moderate oral bioavailability were projected in humans, supporting once daily dosing.

We previously demonstrated that ERα protein turnover may vary across cell lines.³⁶ As such, our first-generation SERD/M 10 promoted increased ERα degradation in an MCF-7 cell line but was much less effective in six other ER+ breast cancer cell lines than 35 (Figure 3). Contrarily, 35 promoted significant

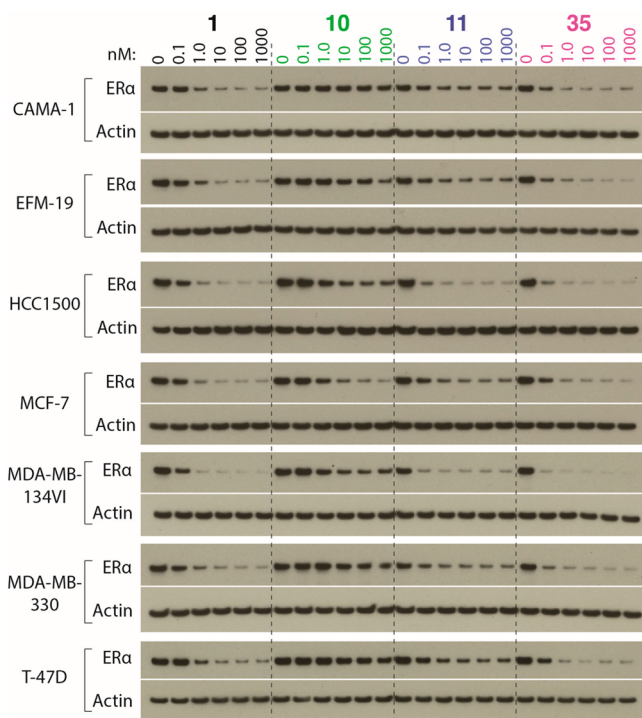


Figure 3. Compound 35 promoted ERα degradation across a panel of ER+ breast cancer cell lines. Cells were treated with 1, 10, 11, and 35 (0.1 nM, 1 nM, 10 nM, 100 nM, or 1 μM) for 24 h.

turnover of ERα across all cell lines tested, starting at the lowest testing concentration of 0.1 nM. In fact, 35 was a more efficient degrader than FDA approved SERD 1 and our second generation SERD 11 in all seven cell lines tested.

We also investigated the degradation kinetics of 35 in comparison to 1, 10, and 11 (Figure 4). In the MCF-7 cell line, 35 promoted the fastest ERα turnover with a half-life of 1.8 h, similar to 1 (2.2 h) and was much faster than 11 (6.0 h) and 10 (16.5 h). In addition, 35 induced the highest ERα degradation at 24 h among the four compounds tested in the Western blot assay.

With robust antagonist and degradation potencies, we evaluated 35 in viability assays across four different ER+ breast cancer cell lines (Figure 5). 35 had comparable potencies to our second-generation SERD 11 across the four cell lines tested. It is also noteworthy that 35 was more potent than FDA-approved SERD 1 and significantly more potent than our first-generation SERD/M 10, illustrating the importance of the mechanism of action related to antagonism and degradation. In general, full antagonists and strong SERDs (11 and 35) were substantially more potent than partial agonists 2a and SERD/M 10. In addition, 35 was more potent than known oral SERDs (6, 7, 9) in viability assays across multiple ER+ breast cancer cell lines (Figure S1 in the Supporting Information).

To evaluate the full antagonist profile, the *in vivo* uterine wet weight (UWW) assay was utilized,⁴⁵ using ethinyl estradiol (EE), 2a, and 11 as controls (Figure 6). Compared to the vehicle control, EE and 2a both increased the ratio of UWW vs body weight significantly by about 3-fold and 2-fold, respectively, indicating ERα agonism (Figure 6a). SERD 11 (10 mg/kg once daily oral dose) reduced the ratio of UWW vs body weight by about 2-fold, indicating ERα antagonism/inverse agonism. Compound 35, at 0.1 mg/kg and 10 mg/kg daily oral doses, reduced the ratio of UWW vs body weight with a statistically significant reduction noted at 10 mg/kg. In addition, the endometrium that lines the uterus was stained using hematoxylin and eosin (H&E) for histological evaluation (Figure 6b). Both EE and 2a, which increased the uterine wet weight, demonstrated a tall columnar phenotype of the epithelial cells. This is in stark contrast to the low cuboidal phenotype of the epithelium observed for the vehicle, 11, and 35. In summary, 35 demonstrated functional inverse agonism *in vivo* using the UWW assay, consistent with our observation in breast cancer cell lines. Collectively, our data confirmed a full antagonist profile for 35 in addition to potentially reduced endometrial cancer risk.

With excellent *in vitro* potency, good ADME properties, and the desired dual mechanism of action profile, 35 was further evaluated in multiple patient derived xenograft (PDX) mouse models. As an example, we evaluated 35 in the HCI-013 PDX tumor model, which harbors both hot-spot Y537S mutant and wild-type ERα (Figure 7). Constitutively active ESR1 mutations such as Y537S in the ligand-binding-domain (LBD) were observed as an acquired resistance mechanism to hormonal therapy such as AIs.^{20–23} Both simulation²⁰ and cocrystal structures^{46,47} revealed a HB formation from the OH group of the mutant residue Ser537 in H12 to Asp351 in H3, thus adopting a stable agonist state which renders resistance to existing endocrine therapies. Therefore, we wondered if a more potent binder might be able to disrupt the HB between Ser537 and Asp351. Approved drug 1 at its clinically relevant dose and our first-generation SERD/M 10 at 100 mg/kg once daily oral

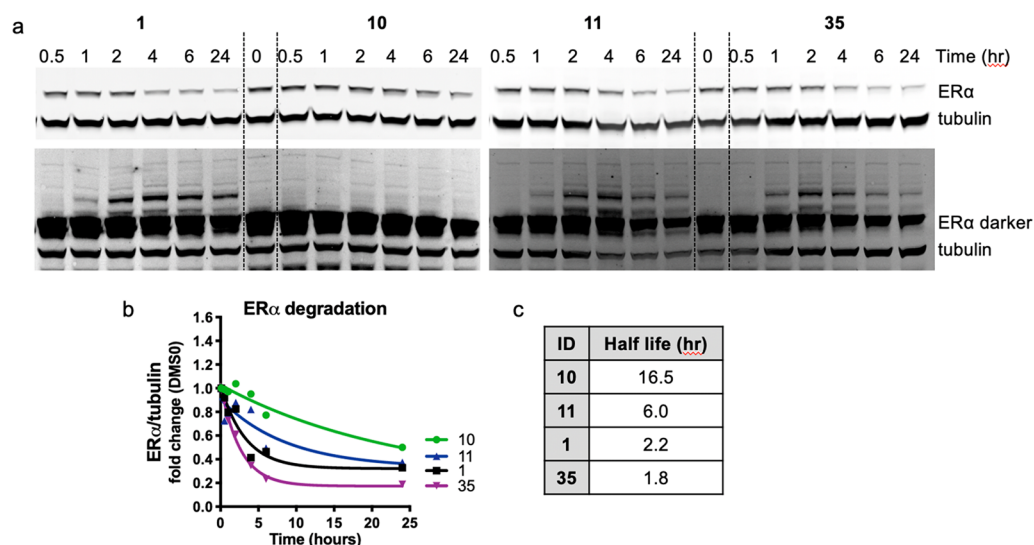


Figure 4. Compound 35 promoted rapid ER α degradation in MCF-7 breast cancer cell lines. (a) Western blot quantifying ER α level at six time points (0.5, 1, 2, 4, 6, 24 h). MCF-7 cells were treated with 1, 10, 11, and 35 at 1 nM. (b) Time course of ER α degradation derived from the Western blot. (c) Half-life of ER α calculated based on the time course for each test compound.

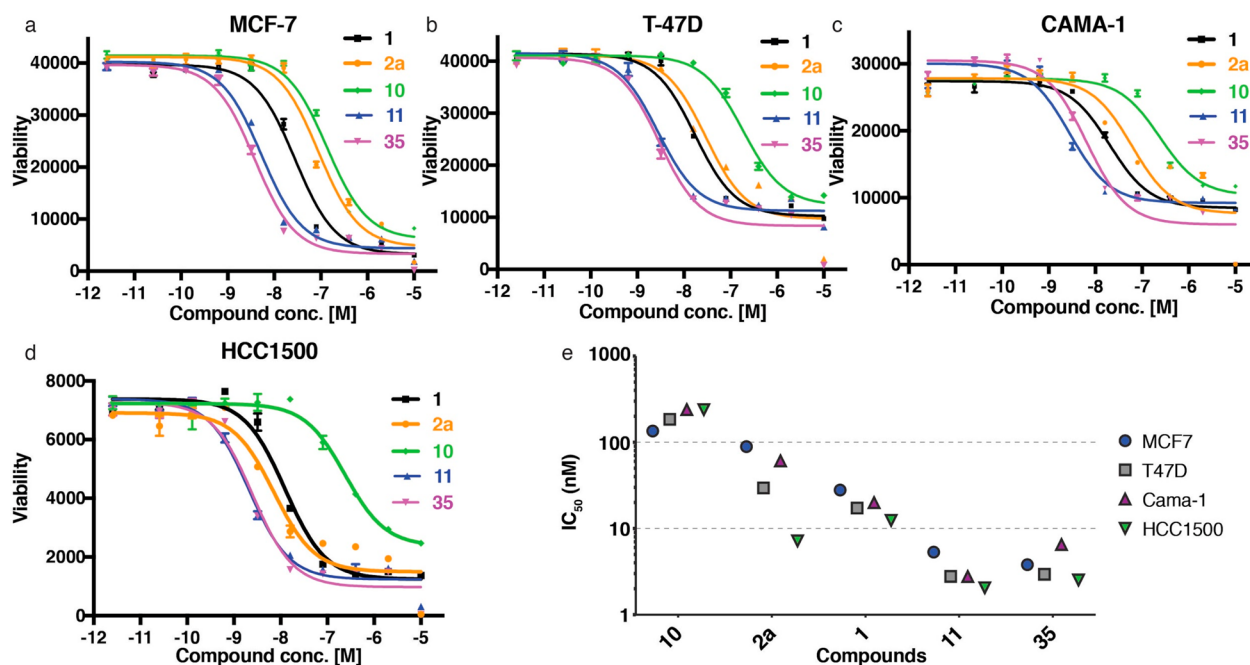


Figure 5. Consistent ER degradation and full ER suppression mediated by 35 resulted in strong activity in cellular viability assays. Dose response curves are displayed measuring cell line viability using CellTiter-Glo at a range of compound concentrations in the (a) MCF-7 breast cancer cell line, (b) T-47D breast cancer cell line, (c) CAMA-1 breast cancer cell line, (d) HCC1500 breast cancer cell line, and (e) anti-proliferation IC₅₀ values of 1, 2a, 10, 11, and 35 in MCF-7, T-47D, CAMA-1, and HCC1500 cell lines.

dose were both efficacious by slowing down the tumor growth, while our second-generation SERD 11 was more efficacious by inducing tumor regression at the 100 mg/kg dose (Figure 7a and Figure S5 in the Supporting Information). Remarkably, 35 could achieve just as robust efficacy as 11, albeit at a 100-fold lower dose (Figure 7b), underscoring the significant improvement in oral exposure and drug potency/efficiency with respect to antagonism and degradation of ER α . In addition, 35 at 1 mg/kg dose had a 10-fold less plasma concentration than 11 at 100 mg/kg, while promoting a 1.8-fold higher ER α turnover (Figure S6 in the Supporting Information). Based on the *in vivo* efficacy data demonstrating tumor regression in the PDX

models, 35 was projected to be efficacious at a low dose (\sim 1 mg, QD) in humans.

CDK4/6 inhibitors such as palbociclib (49) have been approved as combination therapy with either AIs or 1, transforming the landscape of standard of care therapies for ER+ breast cancer.^{8,48,49} We therefore set out to study the combination effect in an MCF-7 mouse xenograft model, harboring wild-type ER α . Dosing of 1 as a single agent at its clinically relevant dose showed resistance in this model, while 49 at 50 mg/kg once daily oral dose delayed the tumor growth by 43% (Figure 8 and Figure S7 in the Supporting Information). A combination of 1 and 49 proved to be similar

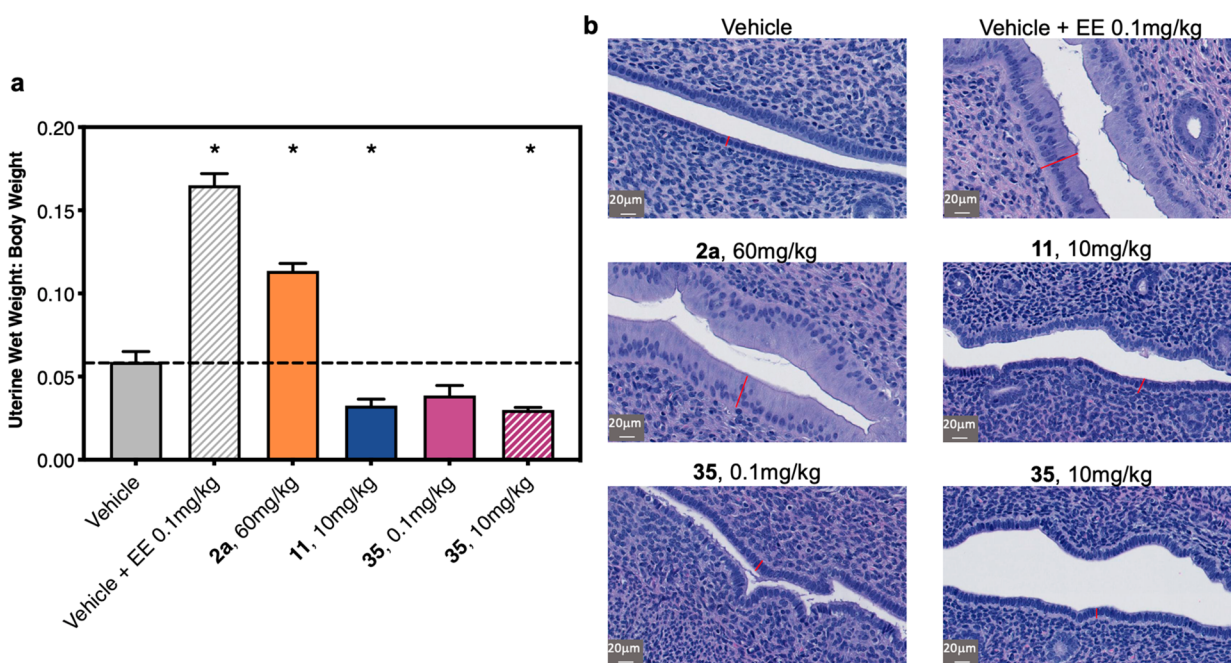


Figure 6. UWW assessment of 35, relative to other controls in immature rats. After oral administration of vehicle (0.5% methylcellulose/0.2% Tween-80), EE (17 α -ethynyl estradiol), 2a, 11, or 35 once daily for 4 days, uterine samples were collected from all groups. (a) Mean (\pm SEM) ratio of uterine weights vs body weight is depicted by the dose group. The black dashed line indicates vehicle mean. Agonism was measured by an increase of the uterine wet weight (UWW) ratio to the body weight. Inverse agonism was measured by a decrease of the UWW ratio. *Denotes significance ($p \leq 0.05$) compared to the vehicle. (b) Histology images are representative of each group with two uterine cross sections examined and three measurements taken from each section ($n = 6$). Height of the surface epithelium of the endometrium is marked with a red line at 20 \times magnification, from the basement membrane to the apical (luminal) surface using an internal digital pathology viewer.

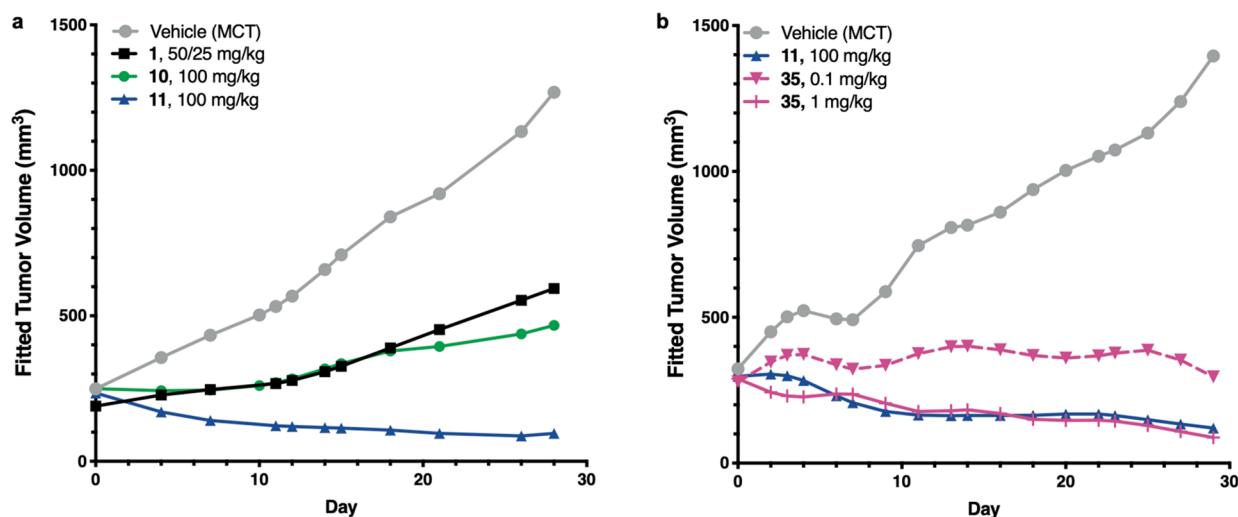


Figure 7. Efficacy of 35 in an HCI-013 PDX breast cancer model harboring an ESR1^{Y537S} mutant. HCI-013 ESR1^{Y537S} PDX tumor bearing mice were dosed once daily orally, except for 1 which was dosed subcutaneously (details in the Supporting Information), with (a) vehicle, 1 (50/25 mg/kg), 10 (100 mg/kg), and 11 (100 mg/kg) for 28 days and (b) vehicle, 11 (100 mg/kg), and 35 (0.1, 1 mg/kg) for 29 days.

to 49 alone in delaying tumor growth. Remarkably, 35 by itself at a suboptimal oral dose of 3 mg/kg once daily inhibited tumor growth by 79%, while combination with 49 caused tumor regression up to 108% after 24 days. All mice tolerated treatment. In summary, 35 demonstrated increased efficacy in combination with a CDK4/6 inhibitor 49 compared to each agent alone in a tumor model that is resistant to 1.

In studies designed to assess the safety of the molecule, 35 was well tolerated in both female rats and female cynomolgus monkeys and displayed an overall favorable safety profile. The

highest nonseverely toxic dose (HNSTD) in a 4-week toxicity study in cynomolgus monkeys, the most sensitive preclinical species, was approximately 190-fold higher than the projected human efficacious exposure based on the HCI-013 ESR1^{Y537S} PDX tumor model. With a favorable *in vitro* and *in vivo* safety profile, we selected 35 as our lead candidate for clinical development.

Synthesis of 35 started with commercially available 2,2-difluoropropane-1,3-diol (50, Scheme 1). Monoprotection of the alcohols with *tert*-butyldiphenylsilyl chloride (TBDPSCI)

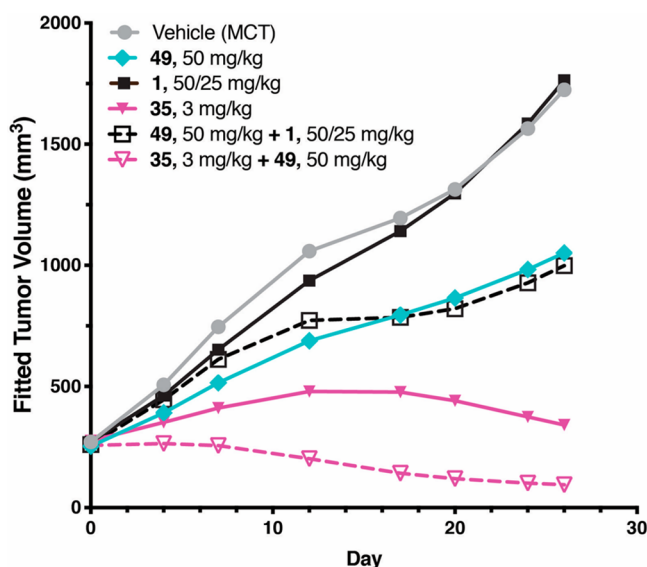
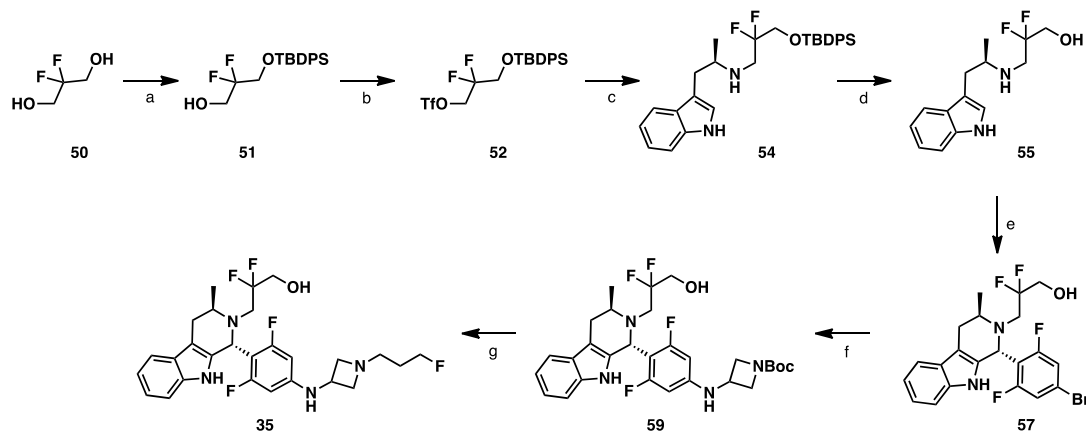


Figure 8. Efficacy of **35** in an MCF-7 xenograft tumor model. MCF-7 tumor bearing mice were dosed once daily orally, except for **1** which was dosed subcutaneously, with vehicle, **1** (50/25 mg/kg), palbociclib (50 mg/kg), **35** (3 mg/kg), a combination of **1** (50/25 mg/kg) and palbociclib (50 mg/kg), or a combination of **35** (3 mg/kg) and palbociclib (50 mg/kg) for 26 days.

gave intermediate **51**, which was subsequently converted to triflate **52** upon reaction with triflic anhydride. *N*-Alkylation of (2*R*)-1-(1*H*-indol-3-yl)propan-2-amine (**53**) with triflate **52** led to compound **54** in excellent yield. Removal of the silyl protecting group in **54**, followed by Pictet–Spengler reaction⁴¹ with 4-bromo-2,6-difluorobenzaldehyde (**56**) yielded intermediate **57** with a *trans*/*cis* ratio of 20:1. **57** was coupled with Boc-protected azetidine (**58**) through a palladium-mediated Buchwald coupling⁵⁰ to give azetidine **59**. Upon removal of the Boc group in **59** with sulfuric acid, the resulting azetidine was *N*-alkylated with 1-fluoro-3-iodopropane (**60**) to give the final compound **35**.

Scheme 1. Synthesis of **35**^a



^aReagents and conditions: (a) TBDPSCl, NaH, THF, 0–20 °C, 72%; (b) Tf₂O, 2,6-lutidine, DCM, 0 °C, 91%; (c) (2*R*)-1-(1*H*-indol-3-yl)propan-2-amine (**53**), DIPEA, 1,4-dioxane, 90 °C, 87%; (d) TBAF, THF, 25 °C, 87%; (e) 4-bromo-2,6-difluorobenzaldehyde (**56**), HOAc, toluene, 90 °C, 71%; (f) *tert*-butyl 3-aminoazetidine-1-carboxylate (**58**), Pd₂(dba)₃, Xantphos, Cs₂CO₃, 1,4-dioxane, 110 °C, 69%; (g) H₂SO₄, 1,4-dioxane, 25 °C; then 1-fluoro-3-iodopropane (**60**), DIPEA, DMF, 25 °C, 15% for two steps.

CONCLUSIONS

We disclose herein a lead optimization effort that resulted in an oral SERD **35** (GDC-9545, giredestrant), whose overall profile is superior to known SERDs and SERMs. Through property- and structure-based drug design, we discovered a polar D-ring replacement, difluoropropyl alcohol, which not only provided multiple interactions with the ERα protein for excellent potency but also modulated the physicochemical properties for a better DMPK profile to enable oral dosing at a low efficacious dose. We carried out a comprehensive SAR effort in driving for maximum degradation efficiency which led to the identification of basic degradation side chains with an NH-azetidine linker. After profiling over 4000 compounds encompassing multiple scaffolds with different mechanisms of action, **35** emerged as our top lead with an overall best profile, including antagonist, degradation, and antiproliferation potency, DMPK properties, and *in vivo* efficacy and safety. In addition to robust single agent activity in xenograft models, **35** in combination with other targeted therapies such as CDK4/6 inhibitors, was well-tolerated and resulted in greater efficacy than each agent alone without any drug–drug interaction liability. **35** is currently being tested in multiple clinical trials including a Phase III trial for locally advanced or metastatic breast cancer treatment (NCT04546009).

EXPERIMENTAL SECTION

All known chemicals (including compounds **1–3**, **6–13**, **49**) and solvents were used directly as received from commercial suppliers or through custom synthesis. Syntheses and characterizations of compounds **14–34** and **36–48** are in the [Supporting Information](#). ¹H NMR spectra were recorded on Bruker Avance 400 or 500 spectrometers. Chemical shifts are expressed in δ ppm referenced to an internal standard, tetramethylsilane (δ = 0 ppm). Abbreviations used in describing peak signals are br = broad signal, s = singlet, d = doublet, dd = doublet of doublets, t = triplet, q = quartet, m = multiplet. All final compounds were purified to have purity higher than 95% by reverse phase high-performance liquid chromatography (HPLC), supercritical fluid chromatography (SFC), or normal phase silica gel chromatography flash chromatography. The purity was assessed by reverse phase HPLC with an isocratic gradient of 5–95% acetonitrile in water (with either acid or base modifier) and

monitored by an ultraviolet diode array detection at wavelength 254 nm. Optical rotation was recorded using an Autopol VI automatic polarimeter from Rudolph Research Analytical. Liquid chromatography mass spectrometry (LCMS) spectra were recorded on a liquid chromatograph–mass spectrometer in electrospray positive (ES+) mode. High-resolution mass spectra (HRMS) experiments were performed on a Dionex LC Ultimate 3000 coupled with a Thermo Scientific Q Exactive Orbitrap mass spectrometer using ESI as the ionization source and a Phenomenex XB-C18, 1.7 mm, 50 mm × 2.1 mm column with a 0.7 mL/min flow rate at 40 °C for liquid chromatography (LC) separation. Solvent A was 0.1% formic acid in water, and solvent B was 0.1% formic acid in acetonitrile. The gradient consisted of 2–98% solvent B over 7 min and held at 98% B for 1.5 min following equilibration for 1.0 min. The LC was monitored by UV absorbance at 220 and 254 nm. MS full scans with 35 000 resolution were applied to all experiments.

3-((*tert*-Butyldiphenylsilyl)oxy)-2,2-difluoropropan-1-ol (51). To a stirred solution of 2,2-difluoropropane-1,3-diol (**50**, 200 mg, 1.78 mmol) in THF (4 mL) on an ice bath was added NaH (60% dispersion in mineral oil, 71 mg, 1.78 mmol), and the reaction mixture was stirred for 30 min. TBDPSCI (490 mg, 1.78 mmol) was added to the reaction mixture dropwise. Then the reaction mixture was warmed up to 20 °C and stirring continued for 3 h. Water (10 mL) was slowly added to the reaction mixture and the resulting mixture was extracted with EtOAc (10 mL × 2). The combined organic layer was dried over anhydrous Na₂SO₄, filtered, and concentrated via rotovap. The crude residue was purified by silica gel column chromatography (20% petroleum ether in EtOAc) to afford the title compound (450 mg, 1.28 mmol, 72% yield) as a light yellow oil. ¹H NMR (400 MHz, CDCl₃) δ 7.71–7.64 (m, 4H), 7.44–7.36 (m, 6H), 3.96–3.84 (m, 4H), 1.86 (s, 1H), 1.06 (s, 9H).

3-((*tert*-Butyldiphenylsilyl)oxy)-2,2-difluoropropyl trifluoromethanesulfonate (52). To a stirred solution of 3-((*tert*-butyl-(diphenyl)silyl)oxy)-2,2-difluoro-propan-1-ol (**51**, 400 mg, 1.14 mmol) and 2,6-lutidine (0.39 mL, 3.42 mmol) in DCM (8 mL) on an ice bath was added Tf₂O (0.38 mL, 2.28 mmol) dropwise. The reaction mixture was stirred at 20 °C for 2 h. The reaction mixture was then poured into ice water (20 mL) slowly, and the mixture was extracted with DCM (20 mL × 2). The combined organic layer was washed with 1 N HCl (20 mL), saturated NaHCO₃ (20 mL), and brine. The organic layer was dried over anhydrous Na₂SO₄, filtered, and concentrated via rotovap. The crude residue was purified by silica gel column chromatography (10% petroleum ether in EtOAc) to afford the desired product (500 mg, 1.04 mmol, 91% yield) as a light yellow oil. ¹H NMR (400 MHz, CDCl₃) δ 7.66–7.64 (m, 4H), 7.47–7.41 (m, 6H), 4.76 (t, *J* = 7.6 Hz, 2H), 3.89 (t, *J* = 7.6 Hz, 2H), 1.08 (s, 9H).

(*R*)-*N*-(1-(1*H*-Indol-3-yl)propan-2-yl)-3-((*tert*-butyldiphenylsilyl)oxy)-2,2-difluoropropan-1-amine (54). A mixture of [3-((*tert*-butyl(diphenyl)silyl)oxy)-2,2-difluoro-propyl] trifluoromethanesulfonate (**52**, 8.31 g, 17.22 mmol), DIPEA (6.1 mL, 34.44 mmol), and (2*R*)-1-(1*H*-indol-3-yl)propan-2-amine (**53**, 3.0 g, 17.22 mmol) in 1,4-dioxane (60 mL) was stirred at 90 °C for 12 h. After being cooled to room temperature, the reaction mixture was diluted with water (100 mL) and was extracted with EtOAc (100 mL × 2). The combined organic layer was dried over anhydrous Na₂SO₄, filtered, and concentrated via rotovap. The crude residue was purified by silica gel column chromatography (20% EtOAc in petroleum ether) to afford the title compound (7.6 g, 87% yield) as a yellow oil. ¹H NMR (400 MHz, CDCl₃) δ 7.90 (br s, 1H), 7.66–7.58 (m, 5H), 7.45–7.31 (m, 7H), 7.20–7.07 (m, 2H), 6.98 (d, *J* = 2.4 Hz, 1H), 3.86–3.78 (m, 2H), 3.21–3.07 (m, 3H), 2.90–2.76 (m, 2H), 1.11 (d, *J* = 6.4 Hz, 3H), 1.04 (s, 9H). LCMS (ESI) *m/z*: 507.2 [*M* + *H*]⁺.

(*R*)-3-((1-(1*H*-Indol-3-yl)propan-2-yl)amino)-2,2-difluoropropan-1-ol (55). To a stirred solution of (*R*)-*N*-(1-(1*H*-indol-3-yl)propan-2-yl)-3-((*tert*-butyldiphenylsilyl)oxy)-2,2-difluoropropan-1-amine (**54**, 7.6 g, 15 mmol) in THF (100 mL) at room temperature was added TBAF (1.0 M in THF, 30 mL, 30 mmol). The reaction mixture was stirred at 25 °C for 4 h, then diluted with water (200 mL), and was extracted with EtOAc (200 mL × 3). The combined

organic layer was dried over anhydrous Na₂SO₄, filtered, and concentrated to dryness. The crude residue was purified by silica gel column chromatography (70% EtOAc in petroleum ether) to afford the title compound (3.5 g, 87% yield) as a light yellow oil. ¹H NMR (600 MHz, CDCl₃) δ 8.06 (br s, 1H), 7.58 (ddd, *J* = 7.9, 1.9, 0.8 Hz, 1H), 7.38 (ddd, *J* = 8.2, 0.9, 0.9 Hz, 1H), 7.21 (ddd, *J* = 8.1, 7.0, 1.2 Hz, 1H), 7.13 (ddd, *J* = 8.0, 7.0, 1.0 Hz, 1H), 7.03 (d, *J* = 2.3 Hz, 1H), 3.91–3.77 (m, 2H), 3.24–3.14 (m, 1H), 3.13–3.03 (m, 2H), 2.90–2.80 (m, 2H), 1.17 (d, *J* = 6.3 Hz, 3H). ¹³C NMR (101 MHz, CDCl₃) δ 136.4, 127.6, 122.6, 122.2, 120.5 (t, ¹*J*_{CF} = 243 Hz), 119.5, 118.8, 112.6, 111.3, 65.1 (t, ²*J*_{CF} = 31 Hz), 53.5, 50.6 (t, ²*J*_{CF} = 29 Hz), 32.9, 20.4. ¹⁹F NMR (CDCl₃, 376 MHz) δ –110.1 (d, *J* = 259.8 Hz), –111.1 (d, *J* = 257.9 Hz). LCMS (ESI) *m/z*: 268.9 [*M* + *H*]⁺.

3-((1*R*,3*R*)-1-(4-Bromo-2,6-difluorophenyl)-3-methyl-3,4-dihydro-1*H*-pyrido[3,4-*b*]indol-2(9*H*)-yl)-2,2-difluoropropan-1-ol (57). A mixture of (*R*)-3-((1-(1*H*-indol-3-yl)propan-2-yl)amino)-2,2-difluoropropan-1-ol (**55**, 20 g, 74.54 mmol), acetic acid (12.91 mL, 223.63 mmol), and 4-bromo-2,6-difluorobenzaldehyde (**56**, 16.47 g, 74.54 mmol) in toluene (400 mL) was stirred at 90 °C for 12 h. The reaction mixture was diluted with water (500 mL) and was extracted with EtOAc (500 mL × 2). The combined organic layer was dried over anhydrous Na₂SO₄, filtered, and concentrated via rotovap. The crude residue was purified by silica gel column chromatography (20% EtOAc in petroleum ether) to afford the title compound (24.8 g, 71% yield, *trans/cis* = 20/1) as a light yellow solid. ¹H NMR (400 MHz, CDCl₃) δ 7.56–7.51 (m, 1H), 7347 (br s, 1H), 7.26–7.22 (m, 1H), 7.19–7.08 (m, 4H), 5.27 (s, 1H), 3.80–3.64 (m, 3H), 3.34–3.19 (m, 1H), 3.14–3.03 (m, 2H), 2.93–2.76 (m, 1H), 2.69 (ddd, *J* = 15.6, 4.3, 1.4 Hz, 1H), 1.19 (d, *J* = 6.6 Hz, 3H). ¹³C NMR (101 MHz, CDCl₃) δ 161.9 (dd, ¹*J*_{CF} = 256.6 Hz, ³*J*_{CF} = 8.2 Hz), 136.4, 129.8, 127.3, 122.8 (t, ³*J*_{CF} = 12.6 Hz), 122.1, 121.4 (t, ¹*J*_{CF} = 245.2 Hz), 119.7, 118.4, 116.3 (d, ²*J*_{CF} = 26.0 Hz), 116.2 (d, ²*J*_{CF} = 26.3 Hz), 115.4 (t, ²*J*_{CF} = 14.5 Hz), 110.9, 108.6, 63.7 (t, ²*J*_{CF} = 30.9 Hz), 52.1 (t, ²*J*_{CF} = 30.2 Hz), 51.6, 51.1, 26.8, 12.6. ¹⁹F NMR (376 MHz, CDCl₃) δ –106.9 (d, *J* = 259.8 Hz), –107.7 (d, *J* = 260.6 Hz), –110.0. LCMS (ESI) *m/z*: 470.9 [*M* + *H*]⁺.

***tert*-Butyl 3-((4-((1*R*,3*R*)-2-(2,2-difluoro-3-hydroxypropyl)-3-methyl-2,3,4,9-tetrahydro-1*H*-pyrido[3,4-*b*]indol-1-yl)-3,5-difluorophenyl)amino)azetidine-1-carboxylate (59).** A mixture of 3-((1*R*,3*R*)-1-(4-bromo-2,6-difluorophenyl)-3-methyl-3,4-dihydro-1*H*-pyrido[3,4-*b*]indol-2(9*H*)-yl)-2,2-difluoropropan-1-ol (**57**, 24.8 g, 52.62 mmol), Pd₂(dba)₃ (4.82 g, 5.26 mmol), Xantphos (6.09 g, 10.52 mmol), Cs₂CO₃ (51.44 g, 157.86 mmol), and *tert*-butyl 3-aminoazetidine-1-carboxylate (**58**, 13.59 g, 78.93 mmol) in 1,4-dioxane (300 mL) was stirred at 110 °C for 3 h under N₂ atmosphere. The reaction mixture was cooled to 25 °C and was diluted with water (500 mL), extracted with EtOAc (500 mL × 2). The combined organic layer was dried over anhydrous Na₂SO₄, filtered, and concentrated. The crude residue was purified by silica gel column chromatography (20% petroleum ether in EtOAc) to afford the title compound (20.5 g, 69% yield, *trans/cis* = 20/1) as a yellow solid. ¹H NMR (400 MHz, CDCl₃) δ 7.68–7.33 (m, 4H), 7.12–7.00 (m, 2H), 5.92 (d, *J* = 12.0 Hz, 2H), 5.03 (s, 1H), 4.62 (dd, *J* = 6.0, 6.0 Hz, 1H), 4.20–3.85 (m, 4H), 3.22–2.53 (m, 7H), 1.36 (s, 9H), 1.07 (d, *J* = 6.5 Hz, 3H). LCMS (ESI) *m/z*: 563.0 [*M* + *H*]⁺.

3-((1*R*,3*R*)-1-(2,6-difluoro-4-((1-(3-fluoropropyl)azetidin-3-yl)amino)phenyl)-3-methyl-1,3,4,9-tetrahydro-2*H*-pyrido[3,4-*b*]indol-2-yl)-2,2-difluoropropan-1-ol (35). To a solution of *tert*-butyl 3-((4-((1*R*,3*R*)-2-(2,2-difluoro-3-hydroxypropyl)-3-methyl-2,3,4,9-tetrahydro-1*H*-pyrido[3,4-*b*]indol-1-yl)-3,5-difluorophenyl)amino)azetidine-1-carboxylate (**59**, 20.5 g, 36.44 mmol) in 1,4-dioxane (194 mL) on an ice bath was added concentrated sulfuric acid (19.42 mL, 364.38 mmol) dropwise. The reaction mixture was stirred at 25 °C for 0.5 h. The reaction mixture was then poured into saturated aqueous NaHCO₃ solution (800 mL) and was extracted with EtOAc (600 mL × 2). The combined organic layer was dried over anhydrous Na₂SO₄, filtered, and concentrated to afford 3-((1*R*,3*R*)-1-(4-(azetidin-3-ylamino)-2,6-difluorophenyl)-3-methyl-3,4-dihydro-1*H*-pyrido[3,4-*b*]indol-2(9*H*)-yl)-2,2-difluoropropan-1-ol

(18.0 g, crude, *trans/cis* = 20/1) as a yellow solid. The crude residue was carried over to the next step directly. ¹H NMR (400 MHz, MeOD): δ 7.39–7.36 (m, 1H), 7.19–7.17 (m, 1H), 7.01–6.92 (m, 2H), 6.13–6.06 (m, 2H), 5.15 (s, 1H), 4.29–4.26 (m, 1H), 3.88–3.59 (m, 4H), 3.31–2.61 (m, 7H), 1.12 (d, *J* = 6.5 Hz, 3H). LCMS (ESI) *m/z*: 463.0 [M + H]⁺.

A mixture of 3-((1*R*,3*R*)-1-(4-(azetidin-3-ylamino)-2,6-difluorophenyl)-3-methyl-3,4-dihydro-1*H*-pyrido[3,4-*b*]indol-2(9*H*)-yl)-2,2-difluoropropan-1-ol (18.0 g, 38.92 mmol), DIPEA (19.3 mL, 116.76 mmol), and 1-fluoro-3-iodopropane (**60**, 7.32 g, 38.92 mmol) in DMF (180 mL) was stirred at 25 °C for 12 h. The reaction mixture was diluted with EtOAc (500 mL) and was washed with brine (500 mL × 3). The combined organic layer was dried over anhydrous Na₂SO₄, filtered, and concentrated via rotovap. The crude residue was purified by silica gel column chromatography (10% MeOH in DCM) to afford the desired product (7.1 g, 85% purity) as a yellow oil. The resulting residue was further purified by reverse phase HPLC (acetonitrile 40–75/0.05% NH₄OH in water) and chiral SFC (AD 250 mm × 50 mm, 10 μm; supercritical CO₂/EtOH (0.1% NH₃·H₂O) = 40/40 at 200 mL/min) to afford the title compound (2.85 g, 15% yield for two steps) as a light yellow solid. ¹H NMR (400 MHz, CD₃OD) δ 7.39 (d, *J* = 7.2 Hz, 1H), 7.19 (d, *J* = 8.0 Hz, 1H), 7.01–6.93 (m, 2H), 6.11 (d, *J* = 12.0 Hz, 2H), 5.16 (s, 1H), 4.52–4.38 (m, 2H), 4.05–4.03 (m, 1H), 3.80–3.74 (m, 3H), 3.63–3.42 (m, 2H), 3.20–3.10 (m, 1H), 2.96–2.92 (m, 3H), 2.82–2.71 (m, 1H), 2.64–2.58 (m, 3H), 1.81–1.68 (m, 2H), 1.14 (d, *J* = 6.4 Hz, 3H). ¹³C NMR (126 MHz, DMSO-*d*₆) δ 164.09, 164.00, 162.14, 162.05, 149.69, 149.57, 149.46, 136.70, 133.22, 127.37, 125.94, 124.01, 122.08, 120.74, 118.53, 117.89, 111.38, 106.66, 103.68, 103.55, 103.42, 95.54, 95.32, 83.16, 81.88, 61.63, 61.17, 60.94, 60.72, 55.32, 55.28, 51.45, 50.91, 50.11, 49.90, 49.68, 43.47, 40.61, 40.52, 40.44, 40.35, 40.27, 40.18, 40.02, 39.85, 39.68, 39.51, 28.82, 28.66, 26.79, 14.45, 0.58. HRMS (ESI) *m/z*: [M + H]⁺ Calcd for C₂₇H₃₂N₄O₅ 523.2491; Found 523.2484.

■ ASSOCIATED CONTENT

Supporting Information

The Supporting Information is available free of charge at <https://pubs.acs.org/doi/10.1021/acs.jmedchem.1c00847>.

Compound properties and characterization, crystallographic data, selectivity, experimental procedures and HPLC-MS spectra, assay protocols, and references (PDF)

Molecular formula strings (CSV)

■ AUTHOR INFORMATION

Corresponding Authors

Jun Liang – Genentech, Inc., South San Francisco, California 94080, United States; orcid.org/0000-0002-6833-0749; Phone: 6504673567; Email: liang.jun@gene.com

Xiaojing Wang – Genentech, Inc., South San Francisco, California 94080, United States; Phone: 6504677959; Email: wang.xiaojing@gene.com

Authors

Jason R. Zbieg – Genentech, Inc., South San Francisco, California 94080, United States; orcid.org/0000-0002-2897-8911

Robert A. Blake – Genentech, Inc., South San Francisco, California 94080, United States

Jae H. Chang – Genentech, Inc., South San Francisco, California 94080, United States; orcid.org/0000-0003-3457-7695

Stephen Daly – Charles River Discovery Research Services UK Limited, Harlow, Essex CM19 5TR, United Kingdom

Antonio G. DiPasquale – Genentech, Inc., South San Francisco, California 94080, United States

Lori S. Friedman – Genentech, Inc., South San Francisco, California 94080, United States

Thomas Gelzleichter – Genentech, Inc., South San Francisco, California 94080, United States

Matthew Gill – Charles River Discovery Research Services UK Limited, Harlow, Essex CM19 5TR, United Kingdom

Jennifer M. Giltane – Genentech, Inc., South San Francisco, California 94080, United States

Simon Goodacre – Charles River Discovery Research Services UK Limited, Harlow, Essex CM19 5TR, United Kingdom

Jane Guan – Genentech, Inc., South San Francisco, California 94080, United States

Steven J. Hartman – Genentech, Inc., South San Francisco, California 94080, United States

Ellen Rei Ingalla – Genentech, Inc., South San Francisco, California 94080, United States

Lorn Kategaya – Genentech, Inc., South San Francisco, California 94080, United States

James R. Kiefer – Genentech, Inc., South San Francisco, California 94080, United States

Tracy Kleinheinz – Genentech, Inc., South San Francisco, California 94080, United States

Sharada S. Labadie – Genentech, Inc., South San Francisco, California 94080, United States

Tommy Lai – WuXi AppTec Co., Ltd., Shanghai 200131, P. R. China

Jun Li – Genentech, Inc., South San Francisco, California 94080, United States

Jiangpeng Liao – WuXi AppTec Co., Ltd., Shanghai 200131, P. R. China

Zhiguo Liu – WuXi AppTec Co., Ltd., Shanghai 200131, P. R. China

Vidhi Mody – Genentech, Inc., South San Francisco, California 94080, United States

Neville McLean – Charles River Discovery Research Services UK Limited, Harlow, Essex CM19 5TR, United Kingdom

Ciara Metcalfe – Genentech, Inc., South San Francisco, California 94080, United States; orcid.org/0000-0001-7233-661X

Michelle A. Nannini – Genentech, Inc., South San Francisco, California 94080, United States

Jason Oeh – Genentech, Inc., South San Francisco, California 94080, United States

Martin G. O'Rourke – Charles River Discovery Research Services UK Limited, Harlow, Essex CM19 5TR, United Kingdom

Daniel F. Ortwine – Genentech, Inc., South San Francisco, California 94080, United States

Yingqing Ran – Genentech, Inc., South San Francisco, California 94080, United States

Nicholas C. Ray – Charles River Discovery Research Services UK Limited, Harlow, Essex CM19 5TR, United Kingdom

Fabien Roussel – Charles River Discovery Research Services UK Limited, Harlow, Essex CM19 5TR, United Kingdom

Amy Sambrone – Genentech, Inc., South San Francisco, California 94080, United States

Deepak Sampath – Genentech, Inc., South San Francisco, California 94080, United States

Leah K. Schutt – Genentech, Inc., South San Francisco, California 94080, United States

Maia Vinogradova – Genentech, Inc., South San Francisco, California 94080, United States

John Wai – WuXi AppTec Co., Ltd., Shanghai 200131, P. R. China

Tao Wang – WuXi AppTec Co., Ltd., Shanghai 200131, P. R. China

Ingrid E. Wertz – Genentech, Inc., South San Francisco, California 94080, United States

Jonathan R. White – Charles River Discovery Research Services UK Limited, Harlow, Essex CM19 5TR, United Kingdom

Siew Kuen Yeap – Charles River Discovery Research Services UK Limited, Harlow, Essex CM19 5TR, United Kingdom

Amy Young – Genentech, Inc., South San Francisco, California 94080, United States

Birong Zhang – Genentech, Inc., South San Francisco, California 94080, United States

Xiaoping Zheng – WuXi AppTec Co., Ltd., Shanghai 200131, P. R. China

Wei Zhou – Genentech, Inc., South San Francisco, California 94080, United States

Yu Zhong – Genentech, Inc., South San Francisco, California 94080, United States

Complete contact information is available at:

<https://pubs.acs.org/10.1021/acs.jmedchem.1c00847>

Author Contributions

The manuscript was written with the help and contributions from all authors. All authors have given approval of the manuscript.

Notes

The authors declare no competing financial interest.

The PDB ID of the new co-crystal structure is 7MSA (35). The authors will release the atomic coordinates upon publication.

ACKNOWLEDGMENTS

Special thanks to Sandra Milan and Jennifer O. Lauchle for strategic discussions and Ria T. Goodwin at Charles River for the assay support. We are grateful to the analytical, purification chemistry, and compound management groups for compound characterization, purification, and handling. Use of the Stanford Synchrotron Radiation Lightsource (SSRL), SLAC National Accelerator Laboratory, is supported by the U.S. Department of Energy, Office of Science, Office of Basic Energy Sciences under Contract No. DE-AC02-76SF00515. The SSRL Structural Molecular Biology Program is supported by the DOE Office of Biological and Environmental Research and by the National Institutes of Health, National Institute of General Medical Sciences (Grant P30GM133894). The contents of this publication are solely the responsibility of the authors and do not necessarily represent the official views of NIGMS or NIH.

ABBREVIATIONS USED

ADME, absorption, distribution, metabolism, and excretion profile; AI, aromatase inhibitors; CO₂, carbon dioxide; DCM, dichloromethane; DIPEA, *N,N*-diisopropylethylamine; DMF, dimethylformamide; DMPK, drug metabolism and pharmacokinetics; EE, ethinyl estradiol; ER α , estrogen receptor α ; ER+, estrogen receptor positive; ES+, electrospray positive; EtOAc, ethyl acetate; HB, hydrogen bond; HCl, hydrogen

chloride; hERG, human ether-à-go-go-related gene; HNR, human nuclear receptors; HPLC, high performance liquid chromatography; HRMS, high-resolution mass spectra; IF, immunofluorescent; LBD, ligand binding domain; LC, liquid chromatography; LC-MS, liquid chromatography-mass spectrometry; LLE, ligand-lipophilicity efficiency; LM, liver microsomes; MCT, methylcellulose tween 80; MDCK, Madin–Darby canine kidney; MeOH, methanol; N₂, nitrogen; Na₂SO₄, sodium sulfate; NaH, sodium hydride; NaHCO₃, sodium bicarbonate; NH₄OH, ammonium hydroxide; NMR, nuclear magnetic resonance; Pd₂(dba)₃, tris-(dibenzylideneacetone)dipalladium(0); PDX, patient derived xenograft; PK, pharmacokinetic; SAR, structure activity relationship; SERD, selective estrogen receptor degrader; SERM, selective estrogen receptor modulator; SFC, supercritical fluid chromatography; S_{inf}, saturation infinity; TBAF, tetra-*N*-butylammonium fluoride; TBDPSCl, *tert*-butyldiphenylsilyl chloride; TDI, time dependent inhibition; THC, tetrahydrocannabinol; THF, tetrahydrofuran; Tf₂O, triflate anhydride; UWW, uterine wet-weight; Xantphos, 4,5-bis-(diphenylphosphino)-9,9-dimethylxanthene.

REFERENCES

- (1) Sung, H.; Ferlay, J.; Siegel, R. L.; Laversanne, M.; Soerjomataram, I.; Jemal, A.; Bray, F. Global Cancer Statistics 2020: GLOBOCAN Estimates of Incidence and Mortality Worldwide for 36 Cancers in 185 Countries. *Ca-Cancer J. Clin.* **2021**, *71*, 209–249.
- (2) Woolston, C. Breast Cancer. *Nature* **2015**, *527* (7578), S101.
- (3) DeSantis, C. E.; Fedewa, S. A.; Goding Sauer, A.; Kramer, J. L.; Smith, R. A.; Jemal, A. Breast Cancer Statistics, 2015: Convergence of Incidence Rates between Black and White Women. *Ca-Cancer J. Clin.* **2016**, *66* (1), 31–42.
- (4) Harvey, J. M.; Clark, G. M.; Osborne, C. K.; Allred, D. C. Estrogen Receptor Status by Immunohistochemistry Is Superior to the Ligand-Binding Assay for Predicting Response to Adjuvant Endocrine Therapy in Breast Cancer. *J. Clin. Oncol.* **1999**, *17* (5), 1474–1481.
- (5) McDonnell, D. P.; Norris, J. D. Connections and Regulation of the Human Estrogen Receptor. *Science* **2002**, *296* (5573), 1642–1644.
- (6) Ariazi, E. A.; Jordan, V. C. *Nuclear Receptors as Drug Targets*; Ottow, E., Weinmann, H., Eds.; Wiley-VCH, 2008; Vol. 39.
- (7) Abderrahman, B.; Jordan, V. C. Successful Targeted Therapies for Breast Cancer: The Worcester Foundation and Future Opportunities in Women's Health. *Endocrinology* **2018**, *159* (8), 2980–2990.
- (8) O'Leary, B.; Finn, R. S.; Turner, N. C. Treating Cancer with Selective CDK4/6 Inhibitors. *Nat. Rev. Clin. Oncol.* **2016**, *13* (7), 417–430.
- (9) Johnston, S. J.; Cheung, K.-L. Endocrine Therapy for Breast Cancer: A Model of Hormonal Manipulation. *Oncol. Ther.* **2018**, *6* (2), 141–156.
- (10) Howell, A.; Osborne, C. K.; Morris, C.; Wakeling, A. E. ICI 182,780 (FaslodexTM). *Cancer* **2000**, *89* (4), 817–825.
- (11) Bross, P. F.; Cohen, M. H.; Williams, G. A.; Pazdur, R. FDA Drug Approval Summaries: Fulvestrant. *Oncologist* **2002**, *7* (6), 477–480.
- (12) Wakeling, A. E.; Dukes, M.; Bowler, J. A Potent Specific Pure Antiestrogen with Clinical Potential. *Cancer Res.* **1991**, *51* (15), 3867–3873.
- (13) van Kruchten, M.; de Vries, E. G.; Glaudemans, A. W.; van Lanschot, M. C.; van Faassen, M.; Kema, I. P.; Brown, M.; Schröder, C. P.; de Vries, E. F.; Hospers, G. A. Measuring Residual Estrogen Receptor Availability during Fulvestrant Therapy in Patients with Metastatic Breast Cancer. *Cancer Discovery* **2015**, *5* (1), 72–81.

- (14) Ohno, S.; Rai, Y.; Iwata, H.; Yamamoto, N.; Yoshida, M.; Iwase, H.; Masuda, N.; Nakamura, S.; Taniguchi, H.; Kamigaki, S.; Noguchi, S. Three Dose Regimens of Fulvestrant in Postmenopausal Japanese Women with Advanced Breast Cancer: Results from a Double-Blind, Phase II Comparative Study (FINDER1). *Ann. Oncol.* **2010**, *21* (12), 2342–2347.
- (15) Jaiyesimi, I. A.; Buzdar, A. U.; Decker, D. A.; Hortobagyi, G. N. Use of Tamoxifen for Breast Cancer: Twenty-Eight Years Later. *J. Clin. Oncol.* **1995**, *13* (2), 513–529.
- (16) Jordan, V. C. Molecular Mechanisms of Antiestrogen Action in Breast Cancer. *Breast Cancer Res. Treat.* **1994**, *31* (1), 41–52.
- (17) Fisher, B.; Costantino, J. P.; Redmond, C. K.; Fisher, E. R.; Wickerham, D. L.; Cronin, W. M.; Other NSABP Contributors. Endometrial Cancer in Tamoxifen-Treated Breast Cancer Patients: Findings From the National Surgical Adjuvant Breast and Bowel Project (NSABP) B-14*. *J. Natl. Cancer Inst.* **1994**, *86* (7), 527–537.
- (18) Gottardis, M. M.; Jordan, V. C. Development of Tamoxifen-Stimulated Growth of MCF-7 Tumors in Athymic Mice after Long-Term Antiestrogen Administration. *Cancer Res.* **1988**, *48* (18), 5183–5187.
- (19) Chang, M. Tamoxifen Resistance in Breast Cancer. *Biomol. Ther.* **2012**, *20* (3), 256–267.
- (20) Toy, W.; Shen, Y.; Won, H.; Green, B.; Sakr, R. A.; Will, M.; Li, Z.; Gala, K.; Fanning, S.; King, T. A.; Hudis, C.; Chen, D.; Taran, T.; Hortobagyi, G.; Greene, G.; Berger, M.; Baselga, J.; Chandarlapaty, S. ESR1 Ligand-Binding Domain Mutations in Hormone-Resistant Breast Cancer. *Nat. Genet.* **2013**, *45* (12), 1439–1445.
- (21) Robinson, D. R.; Wu, Y.-M.; Vats, P.; Su, F.; Lonigro, R. J.; Cao, X.; Kalyana-Sundaram, S.; Wang, R.; Ning, Y.; Hodges, L.; Gursky, A.; Siddiqui, J.; Tomlins, S. A.; Roychowdhury, S.; Pienta, K. J.; Kim, S. Y.; Roberts, J. S.; Rae, J. M.; Van Poznak, C. H.; Hayes, D. F.; Chugh, R.; Kunju, L. P.; Talpaz, M.; Schott, A. F.; Chinnaiyan, A. M. Activating ESR1 Mutations in Hormone-Resistant Metastatic Breast Cancer. *Nat. Genet.* **2013**, *45* (12), 1446–1451.
- (22) Merenbakh-Lamin, K.; Ben-Baruch, N.; Yeheskel, A.; Dvir, A.; Soussan-Gutman, L.; Jeselsohn, R.; Yelensky, R.; Brown, M.; Miller, V. A.; Sarid, D.; Rizel, S.; Klein, B.; Rubinek, T.; Wolf, I. D538G Mutation in Estrogen Receptor- α : A Novel Mechanism for Acquired Endocrine Resistance in Breast Cancer. *Cancer Res.* **2013**, *73* (23), 6856–6864.
- (23) Jeselsohn, R.; Yelensky, R.; Buchwalter, G.; Frampton, G.; Meric-Bernstam, F.; Gonzalez-Angulo, A. M.; Ferrer-Lozano, J.; Perez-Fidalgo, J. A.; Cristofanilli, M.; Gómez, H.; Arteaga, C. L.; Giltane, J.; Balko, J. M.; Cronin, M. T.; Jarosz, M.; Sun, J.; Hawryluk, M.; Lipson, D.; Otto, G.; Ross, J. S.; Dvir, A.; Soussan-Gutman, L.; Wolf, I.; Rubinek, T.; Gilmore, L.; Schnitt, S.; Come, S. E.; Pusztai, L.; Stephens, P.; Brown, M.; Miller, V. A. Emergence of Constitutively Active Estrogen Receptor- α Mutations in Pretreated Advanced Estrogen Receptor-Positive Breast Cancer. *Clin. Cancer Res.* **2014**, *20* (7), 1757–1767.
- (24) De Savi, C.; Bradbury, R. H.; Rabow, A. A.; Norman, R. A.; de Almeida, C.; Andrews, D. M.; Ballard, P.; Buttar, D.; Callis, R. J.; Currie, G. S.; Curwen, J. O.; Davies, C. D.; Donald, C. S.; Feron, L. J. L.; Gingell, H.; Glossop, S. C.; Hayter, B. R.; Hussain, S.; Karoutchi, G.; Lamont, S. G.; MacFaul, P.; Moss, T. A.; Pearson, S. E.; Tonge, M.; Walker, G. E.; Weir, H. M.; Wilson, Z. Optimization of a Novel Binding Motif to (E)-3-(3,5-Difluoro-4-((1R,3R)-2-(2-Fluoro-2-methylpropyl)-3-methyl-2,3,4,9-tetrahydro-1H-pyrido[3,4-b]indol-1-yl)phenyl)acrylic Acid (AZD9496), a Potent and Orally Bioavailable Selective Estrogen Receptor Downregulator and Antagonist. *J. Med. Chem.* **2015**, *58* (20), 8128–8140.
- (25) Tria, G. S.; Abrams, T.; Baird, J.; Burks, H. E.; Firestone, B.; Gaither, L. A.; Hamann, L. G.; He, G.; Kirby, C. A.; Kim, S.; Lombardo, F.; Macchi, K. J.; McDonnell, D. P.; Mishina, Y.; Norris, J. D.; Nunez, J.; Springer, C.; Sun, Y.; Thomsen, N. M.; Wang, C.; Wang, J.; Yu, B.; Tiong-Yip, C.-L.; Peukert, S. Discovery of LSZ102, a Potent, Orally Bioavailable Selective Estrogen Receptor Degradator (SERD) for the Treatment of Estrogen Receptor Positive Breast Cancer. *J. Med. Chem.* **2018**, *61* (7), 2837–2864.
- (26) Andreano, K. J.; Wardell, S. E.; Baker, J. G.; Desautels, T. K.; Baldi, R.; Chao, C. A.; Heetderks, K. A.; Bae, Y.; Xiong, R.; Tonetti, D. A.; Gutgesell, L. M.; Zhao, J.; Sorrentino, J. A.; Thompson, D. A.; Bisi, J. E.; Strum, J. C.; Thatcher, G. R. J.; Norris, J. D. G1T48, an Oral Selective Estrogen Receptor Degradator, and the CDK4/6 Inhibitor Lerociclib Inhibit Tumor Growth in Animal Models of Endocrine-Resistant Breast Cancer. *Breast Cancer Res. Treat.* **2020**, *180* (3), 635–646.
- (27) Garner, F.; Shomali, M.; Paquin, D.; Lyttle, C. R.; Hattersley, G. RAD1901: A Novel, Orally Bioavailable Selective Estrogen Receptor Degradator That Demonstrates Antitumor Activity in Breast Cancer Xenograft Models. *Anti-Cancer Drugs* **2015**, *26* (9), 948–956.
- (28) Bihani, T.; Patel, H. K.; Arlt, H.; Tao, N.; Jiang, H.; Brown, J. L.; Purandare, D. M.; Hattersley, G.; Garner, F. Elacestrant (RAD1901), a Selective Estrogen Receptor Degradator (SERD), Has Antitumor Activity in Multiple ER(+) Breast Cancer Patient-Derived Xenograft Models. *Clin. Cancer Res.* **2017**, *23* (16), 4793–4804.
- (29) Scott, J. S.; Moss, T. A.; Balazs, A.; Barlaam, B.; Breed, J.; Carbajo, R. J.; Chiarpin, E.; Davey, P. R. J.; Delpuech, O.; Fawell, S.; Fisher, D. I.; Gargic, S.; Gangl, E. T.; Grebe, T.; Greenwood, R. D.; Hande, S.; Hatoum-Mokdad, H.; Herlihy, K.; Hughes, S.; Hunt, T. A.; Huynh, H.; Janbon, S. L. M.; Johnson, T.; Kavanagh, S.; Klinowska, T.; Lawson, M.; Lister, A. S.; Marden, S.; McGinnity, D. F.; Morrow, C. J.; Nissink, J. W. M.; O'Donovan, D. H.; Peng, B.; Polanski, R.; Stead, D. S.; Stokes, S.; Thakur, K.; Throner, S. R.; Tucker, M. J.; Varnes, J.; Wang, H.; Wilson, D. M.; Wu, D.; Wu, Y.; Yang, B.; Yang, W. Discovery of AZD9833, a Potent and Orally Bioavailable Selective Estrogen Receptor Degradator and Antagonist. *J. Med. Chem.* **2020**, *63* (23), 14530–14559.
- (30) Smith, P. G.; Puyang, X.; Furman, C.; Zheng, G. Z.; Banka, D.; Thomas, M.; Subramanian, V.; Irwin, S.; Larsen, N.; Caleb, B.; Karr, C.; Wu, J.; O'Shea, M.; Yang, J.; Davis, A.; Kim, A.; Rioux, N.; Rimmunas, V.; Yao, H.; MacKenzie, C.; Kumar, P.; Smith, S.; Eckley, S.; Hart, A.; Lai, G.; Rowbottom, C.; Fekkes, P.; Buonamici, S.; Reynolds, D.; Yu, L.; Sahmoud, T.; Warmuth, M.; Mitchell, L.; Zhu, P.; Korpil, M. Abstract DDT01-04: Discovery and Development of H3B-6545: A Novel, Oral, Selective Estrogen Receptor Covalent Antagonist (SERCA) for the Treatment of Breast Cancer. *Cancer Res.* **2017**, *77* (13 Supplement), DDT01-04.
- (31) Rioux, N.; Smith, S.; Korpil, M.; O'Shea, M.; Prajapati, S.; Zheng, G. Z.; Warmuth, M.; Smith, P. G. Nonclinical Pharmacokinetics and in Vitro Metabolism of H3B-6545, a Novel Selective ER α Covalent Antagonist (SERCA). *Cancer Chemother. Pharmacol.* **2019**, *83* (1), 151–160.
- (32) El-Ahmad, Y.; Tabart, M.; Halley, F.; Certal, V.; Thompson, F.; Filoche-Rommé, B.; Gruss-Leleu, F.; Muller, C.; Brollo, M.; Fabien, L.; Loyau, V.; Bertin, L.; Richepin, P.; Pilorge, F.; Desmazeau, P.; Girardet, C.; Beccari, S.; Louboutin, A.; Lebourg, G.; Le-Roux, J.; Terrier, C.; Vallée, F.; Steier, V.; Mathieu, M.; Rak, A.; Abecassis, P.-Y.; Vicat, P.; Benard, T.; Bouaboula, M.; Sun, F.; Shomali, M.; Hebert, A.; Levit, M.; Cheng, H.; Courjaud, A.; Ginesty, C.; Perrault, C.; Garcia-Echeverria, C.; McCort, G.; Schio, L. Discovery of 6-(2,4-Dichlorophenyl)-5-[4-[(3 S)-1-(3-Fluoropropyl)pyrrolidin-3-yl]-oxyphenyl]-8,9-dihydro-7 H -Benzo[7]Annulene-2-Carboxylic Acid (SAR439859), a Potent and Selective Estrogen Receptor Degradator (SERD) for the Treatment of Estrogen-Receptor-Positive Breast Cancer. *J. Med. Chem.* **2020**, *63* (2), 512–528.
- (33) Lai, A.; Kahraman, M.; Govek, S.; Nagasawa, J.; Bonnefous, C.; Julien, J.; Douglas, K.; Sensintaffar, J.; Lu, N.; Lee, K.-J.; Aparicio, A.; Kaufman, J.; Qian, J.; Shao, G.; Prudente, R.; Moon, M. J.; Joseph, J. D.; Darimont, B.; Brigham, D.; Grillot, K.; Heyman, R.; Rix, P. J.; Hager, J. H.; Smith, N. D. Identification of GDC-0810 (ARN-810), an Orally Bioavailable Selective Estrogen Receptor Degradator (SERD) That Demonstrates Robust Activity in Tamoxifen-Resistant Breast Cancer Xenografts. *J. Med. Chem.* **2015**, *58* (12), 4888–4904.
- (34) Carlson, R. H. Estrogen-Receptor Degradator GDC-0810 Active in Metastatic Breast Cancer. *Oncol. Times* **2015**, *37* (11), 32–33.
- (35) Savage, S.; McClory, A.; Zhang, H.; Cravillon, T.; Lim, N. K.; Masui, C.; Robinson, S. J.; Han, C.; Ochs, C.; Rege, P. D.; Gosselin, F.

Synthesis of Selective Estrogen Receptor Degradator GDC-0810 via Stereocontrolled Assembly of a Tetrasubstituted All-Carbon Olefin. *J. Org. Chem.* **2018**, 83 (19), 11571–11576.

(36) Joseph, J. D.; Darimont, B.; Zhou, W.; Arrazate, A.; Young, A.; Ingalla, E.; Walter, K.; Blake, R. A.; Nonomiya, J.; Guan, Z.; Kategaya, L.; Govek, S. P.; Lai, A. G.; Kahraman, M.; Brigham, D.; Sensintaffar, J.; Lu, N.; Shao, G.; Qian, J.; Grillot, K.; Moon, M.; Prudente, R.; Bischoff, E.; Lee, K.-J.; Bonnefous, C.; Douglas, K. L.; Julien, J. D.; Nagasawa, J. Y.; Aparicio, A.; Kaufman, J.; Haley, B.; Giltane, J. M.; Wertz, I. E.; Lackner, M. R.; Nannini, M. A.; Sampath, D.; Schwarz, L.; Manning, H. C.; Tantawy, M. N.; Arteaga, C. L.; Heyman, R. A.; Rix, P. J.; Friedman, L.; Smith, N. D.; Metcalfe, C.; Hager, J. H. The Selective Estrogen Receptor Downregulator GDC-0810 Is Efficacious in Diverse Models of ER+ Breast Cancer. *eLife* **2016**, 5, 1535.

(37) Kahraman, M.; Govek, S. P.; Nagasawa, J. Y.; Lai, A.; Bonnefous, C.; Douglas, K.; Sensintaffar, J.; Liu, N.; Lee, K.; Aparicio, A.; Kaufman, J.; Qian, J.; Shao, G.; Prudente, R.; Joseph, J. D.; Darimont, B.; Brigham, D.; Heyman, R.; Rix, P. J.; Hager, J. H.; Smith, N. D. Maximizing ER- α Degradation Maximizes Activity in a Tamoxifen-Resistant Breast Cancer Model: Identification of GDC-0927. *ACS Med. Chem. Lett.* **2019**, 10 (1), 50–55.

(38) Edwards, M. P.; Price, D. A. Chapter 23 Role of Physicochemical Properties and Ligand Lipophilicity Efficiency in Addressing Drug Safety Risks. *Annu. Rep. Med. Chem.* **2010**, 45, 380–391.

(39) Liang, J.; Blake, R.; Chang, J.; Friedman, L. S.; Goodacre, S.; Hartman, S.; Ingalla, E. R.; Kiefer, J. R.; Kleinheinz, T.; Labadie, S.; Li, J.; Lai, K. W.; Liao, J.; Mody, V.; McLean, N.; Metcalfe, C.; Nannini, M.; Otwine, D.; Ran, Y.; Ray, N.; Roussel, F.; Sambrone, A.; Sampath, D.; Vinogradova, M.; Wai, J.; Wang, T.; Yeap, K.; Young, A.; Zbieg, J.; Zhang, B.; Zheng, X.; Zhong, Y.; Wang, X. Discovery of GNE-149 as a Full Antagonist and Efficient Degradator of Estrogen Receptor Alpha for ER+ Breast Cancer. *ACS Med. Chem. Lett.* **2020**, 11 (6), 1342–1347.

(40) Leeson, P. D.; Springthorpe, B. The Influence of Drug-like Concepts on Decision-Making in Medicinal Chemistry. *Nat. Rev. Drug Discovery* **2007**, 6 (11), 881–890.

(41) Youn, S. W. THE PICTET-SPENGLER REACTION: EFFICIENT CARBON-CARBON BOND FORMING REACTION IN HETEROCYCLIC SYNTHESIS. *Org. Prep. Proced. Int.* **2006**, 38 (6), 505–591.

(42) Guan, J.; Zhou, W.; Hafner, M.; Blake, R. A.; Chalouni, C.; Chen, I. P.; De Bruyn, T.; Giltane, J. M.; Hartman, S. J.; Heidersbach, A.; Houtman, R.; Ingalla, E.; Kategaya, L.; Kleinheinz, T.; Li, J.; Martin, S. E.; Modrusan, Z.; Nannini, M.; Oeh, J.; Ubhayakar, S.; Wang, X.; Wertz, I. E.; Young, A.; Yu, M.; Sampath, D.; Hager, J. H.; Friedman, L. S.; Daemen, A.; Metcalfe, C. Therapeutic Ligands Antagonize Estrogen Receptor Function by Impairing Its Mobility. *Cell* **2019**, 178 (4), 949–963.e18.

(43) Labadie, S. S.; Li, J.; Blake, R. A.; Chang, J. H.; Goodacre, S.; Hartman, S. J.; Liang, W.; Kiefer, J. R.; Kleinheinz, T.; Lai, T.; Liao, J.; Ortwine, D. F.; Mody, V.; Ray, N. C.; Roussel, F.; Vinogradova, M.; Yeap, S. K.; Zhang, B.; Zheng, X.; Zbieg, J. R.; Liang, J.; Wang, X. Discovery of a C-8 Hydroxychromene as a Potent Degradator of Estrogen Receptor Alpha with Improved Rat Oral Exposure over GDC-0927. *Bioorg. Med. Chem. Lett.* **2019**, 29 (16), 2090–2093.

(44) Liu, Y.-T.; Hao, H.-P.; Liu, C.-X.; Wang, G.-J.; Xie, H.-G. Drugs as CYP3A Probes, Inducers, and Inhibitors. *Drug Metab. Rev.* **2007**, 39 (4), 699–721.

(45) Jordan, V. C.; Gosden, B. Differential Antiestrogen Action in the Immature Rat Uterus: A Comparison of Hydroxylated Antiestrogens with High Affinity for the Estrogen Receptor. *J. Steroid Biochem.* **1983**, 19 (3), 1249–1258.

(46) Nettles, K. W.; Bruning, J. B.; Gil, G.; Nowak, J.; Sharma, S. K.; Hahn, J. B.; Kulp, K.; Hochberg, R. B.; Zhou, H.; Katzenellenbogen, J. A.; Katzenellenbogen, B. S.; Kim, Y.; Joachimiak, A.; Greene, G. L. NF κ B Selectivity of Estrogen Receptor Ligands Revealed by Comparative Crystallographic Analyses. *Nat. Chem. Biol.* **2008**, 4 (4), 241–247.

(47) Fanning, S. W.; Mayne, C. G.; Dharmarajan, V.; Carlson, K. E.; Martin, T. A.; Novick, S. J.; Toy, W.; Green, B.; Panchamukhi, S.; Katzenellenbogen, B. S.; Tajkhorshid, E.; Griffin, P. R.; Shen, Y.; Chandralapathy, S.; Katzenellenbogen, J. A.; Greene, G. L. Estrogen Receptor Alpha Somatic Mutations Y537S and D538G Confer Breast Cancer Endocrine Resistance by Stabilizing the Activating Function-2 Binding Conformation. *eLife* **2016**, 5, e12792.

(48) Turner, N. C.; Slamon, D. J.; Ro, J.; Bondarenko, I.; Im, S.-A.; Masuda, N.; Colleoni, M.; DeMichele, A.; Loi, S.; Verma, S.; Iwata, H.; Harbeck, N.; Loibl, S.; Andre, F.; Puyana Theall, K.; Huang, X.; Giorgetti, C.; Huang Bartlett, C.; Cristofanilli, M. Overall Survival with Palbociclib and Fulvestrant in Advanced Breast Cancer. *N. Engl. J. Med.* **2018**, 379 (20), 1926–1936.

(49) Finn, R. S.; Martin, M.; Rugo, H. S.; Jones, S.; Im, S.-A.; Gelmon, K.; Harbeck, N.; Lipatov, O. N.; Walshe, J. M.; Moulder, S.; Gauthier, E.; Lu, D. R.; Randolph, S.; Diéras, V.; Slamon, D. J. Palbociclib and Letrozole in Advanced Breast Cancer. *N. Engl. J. Med.* **2016**, 375 (20), 1925–1936.

(50) Forero-Cortés, P. A.; Haydl, A. M. The 25th Anniversary of the Buchwald–Hartwig Amination: Development, Applications, and Outlook. *Org. Process Res. Dev.* **2019**, 23 (8), 1478–1483.